

Agost Tasi*, Xavier Gaona*, David Fellhauer, Melanie Böttle, Jörg Rothe, Kathy Dardenne, Dieter Schild, Mireia Grivé, Elisenda Colàs, Jordi Bruno, Klas Källström, Marcus Altmaier and Horst Geckeis

Redox behavior and solubility of plutonium under alkaline, reducing conditions

<https://doi.org/10.1515/ract-2017-2870>

Received August 24, 2017; accepted October 27, 2017; published online January 20, 2018

Abstract: The solubility and redox behavior of hydrous Pu(IV) oxide was comprehensively investigated by an experimental multi-method approach as a function of different redox conditions in 0.1 M NaCl solutions, allowing a detailed characterization of Pu(IV) and Pu(III) solubility and solid phase stability in these systems. Samples were prepared at $-3 \leq \text{pH}_m \leq -6$ ($\text{pH}_m = -\log m_H$) and $-8 \leq \text{pH}_m \leq -13$ at $T = (22 \pm 2)^\circ\text{C}$ under Ar atmosphere. No redox buffer was used in one set of samples, whereas mildly and strongly reducing redox conditions were buffered in two series with hydroquinone or SnCl_2 , respectively, resulting in $(\text{pe} + \text{pH}_m) = (9.5 \pm 1)$ and (2 ± 1) . XRD, XANES and EXAFS confirmed the predominance of Pu(IV) and the nanocrystalline character of the original, aged $\text{PuO}_2(\text{ncr,hyd})$ solid phase used as a starting material. Rietveld analysis of the XRD data indicated an average crystal (domain) size of (4 ± 1) nm with a mean cell parameter of (5.405 ± 0.005) Å. The solubility constant of this solid phase was determined as $\log^* K_{s,0}^\circ = -(58.1 \pm 0.3)$ combining solubility data in acidic conditions and redox speciation by solvent extraction and CE–SF–ICP–MS. This value is in excellent agreement with the current thermodynamic selection in the NEA-TDB. Synchrotron-based *in-situ* XRD, XANES and EXAFS indicate that $\text{PuO}_2(\text{ncr,hyd})$ is the solid phase controlling the solubility of Pu in hydroquinone buffered samples. Under these redox conditions and $-8 \leq \text{pH}_m \leq -13$, the solubility of Pu is very low

($\sim 10^{-10.5}$ m) and pH-independent. This is consistent with the solubility equilibrium $\text{PuO}_2(\text{am,hyd}) + 2\text{H}_2\text{O}(\text{l}) \leftrightarrow \text{Pu}(\text{OH})_4(\text{aq})$. Although *in-situ* XRD unequivocally shows the predominance of PuO_2 in Sn(II)-buffered systems, XANES analyses indicate a significant contribution of Pu(III) ($30 \pm 5\%$) in the solid phases controlling the solubility of Pu at $(\text{pe} + \text{pH}_m) = (2 \pm 1)$. For this system, EXAFS shows a systematic shortening of Pu–O and Pu–Pu distances compared to the starting Pu material and hydroquinone-buffered systems. The solubility of Pu remains very low ($\sim 10^{-10.5}$ m) at $\text{pH}_m > 9$, but shows a very large scattering ($\sim 10^{-9}$ – $10^{-10.5}$ m) at $\text{pH}_m = 8$. Experimental observations collected in Sn(II) buffered systems can be explained by the co-existence of both $\text{PuO}_2(\text{ncr,hyd})$ and $\text{Pu}(\text{OH})_3(\text{am})$ solid phases, but also by assuming the formation of a sub-stoichiometric $\text{PuO}_{2-x}(\text{s})$ phase. This extensive study provides robust upper limits for Pu solubility in alkaline, mildly to strongly reducing conditions relevant in the context of nuclear waste disposal. The potential role of Pu(III) in the solid phases controlling the solubility of Pu under these conditions is analysed and discussed in view of the current NEA-TDB thermodynamic selection, which supports the predominance of $\text{PuO}_2(\text{am,hyd})$ and constrains the formation of $\text{Pu}(\text{OH})_3(\text{am})$ at $\text{pH}_m > 8$ outside the stability field of water.

Keywords: Plutonium, Pu(IV), Pu(III), solubility, alkaline, reducing conditions, thermodynamics.

1 Introduction

A thorough knowledge of the aquatic chemistry and thermodynamics of actinides is fundamental for the long-term safety assessment of repositories for nuclear waste disposal. The internationally favored option for the final disposal of nuclear waste is based upon emplacing waste in deep geological formations where strongly reducing conditions are expected to develop in the post-closure period. In the case of low and intermediate level waste (L/ILW), the use of cementitious materials for the stabilization of the waste and for construction purposes is frequently considered. The interaction of cement-based materials with

*Corresponding authors: Agost Tasi and Xavier Gaona, Karlsruhe Institute of Technology, Institute for Nuclear Waste Disposal, P.O. Box 3640, 76021 Karlsruhe, Germany, E-mail: agost.tasi@kit.edu (A. Tasi); xavier.gaona@kit.edu (X. Gaona)

David Fellhauer, Melanie Böttle, Jörg Rothe, Kathy Dardenne, Dieter Schild, Marcus Altmaier and Horst Geckeis: Karlsruhe Institute of Technology, Institute for Nuclear Waste Disposal, P.O. Box 3640, 76021 Karlsruhe, Germany

Mireia Grivé, Elisenda Colàs and Jordi Bruno: Amphos21 Consulting S.L., Passeig de Garcia i Fària, 49-51, 1^o-1^a, E08019 Barcelona, Spain
Klas Källström: Svensk Kärnbränslehantering AB, avd. Avfall och Rivning, Box 250, 101 24 Stockholm, Sweden

water buffers pH in the alkaline to hyperalkaline range ($10 \leq \text{pH} \leq 13.3$) over long time-scales. This is also expected for the low and intermediate level waste repository SFR of SKB, Swedish Nuclear Fuel and Waste Management Company in Sweden [1], in which context the present study was performed.

Although plutonium is not abundant in SFR, there are significant amounts present which contribute to the long-term risk as a result of the long half-life of ^{239}Pu ($t_{1/2} = 2.41 \cdot 10^4 \text{ a}$) [1]. An important issue with the chemical behavior of plutonium is related to the several different redox states in which the element can exist. In aqueous media, four oxidation states of plutonium are thermodynamically stable, namely +III, +IV, +V and +VI. Amongst these, the predominance of Pu(III) and Pu(IV) is expected under repository relevant, reducing conditions [2].

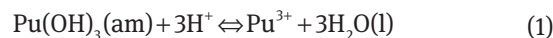
The thermochemical database (TDB) project of the Nuclear Energy Agency (OECD-NEA) contains the most comprehensive and reliable selection of thermodynamic data currently available [3–5] for actinides and fission products. In the last NEA-TDB update volume [5] on Pu data, relevant limitations and uncertainties were reported for the selection of thermodynamic data for Pu aqueous species and solid phases forming under alkaline and reducing conditions. The propagation of the given uncertainties leads to a rather ill-defined Pu(IV)/Pu(III) redox transition, which strongly affects the correct prediction of solubility and chemical behavior of Pu under these conditions.

1.1 Discussion of previous experimental studies

Only few experimental studies that deal with the solubility and hydrolysis of Pu under reducing conditions are reported. This is especially critical under alkaline to hyperalkaline pH conditions, where very limited data [6] are available below $(\text{pe} + \text{pH}) = 4$. This framework introduces relevant uncertainties in the thermodynamic data derived for Pu(III) aqueous species and solid compounds forming in this pH-range, and conversely to the redox transition Pu(IV)/Pu(III). The most relevant investigations on this system available in the literature are discussed in the following.

Felmy et al. [7] investigated the solubility of $\text{Pu}(\text{OH})_3(\text{am})$ within $6.5 \leq -\log [\text{H}^+] \leq 13$ in deionized water and in chloride brines. Redox conditions were buffered by the presence of Fe(0) powder. E_h values were only reported for the pH-range $6.6 \leq -\log [\text{H}^+] \leq 8.1$, and confirmed the strong reducing conditions imposed by Fe

with $(\text{pe} + \text{pH}) = (2 \pm 1)$. Experimental solubility data at $-\log [\text{H}^+] \geq 9$ were below the detection limit of liquid scintillation counting (LSC), and thus were disregarded in the thermodynamic interpretation by the authors. Data at $-\log [\text{H}^+] < 9$ were used to derive $\log {}^*K_{s,0}^\circ$ for the solubility reaction (1) assuming that only non-hydrolysed $\text{Pu}^{3+}(\text{aq})$ species formed below this pH:



NEA-TDB [4] accepted the reported solubility product ($\log {}^*K_{s,0}^\circ = 15.8$), but assigned a very large uncertainty ($\pm 1.5 \log_{10}$ -units) to account for the large uncertainties in the pH measurements and the steep slope of the solubility curve in the investigated pH-range. Besides the uncertainties in pH, other relevant shortcomings appear in the study of Felmy and co-workers. The solubility limiting solid phase was not characterized but assumed to be $\text{Pu}(\text{OH})_3(\text{am})$. As indicated in Neck et al. [2], the oxidation of this solid phase to $\text{PuO}_2(\text{am,hyd})$ cannot be ruled out, especially considering the drop in solubility at $-\log [\text{H}^+] \geq 7$ and the experimental $(\text{pe} + \text{pH})$ values which were rather in the stability field of $\text{PuO}_2(\text{am,hyd})$. The $\log {}^*K_{s,0}^\circ$ reported in Lemire et al. [4] is also not consistent with the thermodynamic model provided by the NEA-TDB selection, which foresees the predominance of PuOH^{2+} instead of Pu^{3+} above $-\log [\text{H}^+] \approx 7$. Yet, these shortcomings are acknowledged by the large uncertainty assigned by the NEA-TDB, and the work by Felmy and co-workers remains as the most reliable solubility study on $\text{Pu}(\text{OH})_3(\text{am})$ published to date.

Nilsson et al. [8] studied the solubility of Pu at $3 \leq \text{pH} \leq 10$ in autoclaves with a pressure of 50 bar $\text{H}_2(\text{g})$ containing a small piece of Pt wire. $\text{Pu}(\text{OH})_3(\text{am})$ was expected to control the solubility of Pu under these strongly reducing conditions. While the blue solid phase initially precipitated by the authors supported this hypothesis, the change in color towards a greenish phase and the unexpectedly low Pu concentration suggested the formation of a PuO_2 solid phase and a solubility equilibrium governed by the reductive dissolution of PuO_2 according to $\text{Pu}(\text{IV})_s + e^- \rightleftharpoons \text{Pu}(\text{III})_{\text{aq}}$. This was also consistent with the mildly reducing redox potentials measured by the authors at the end of their experiments, $(\text{pe} + \text{pH}) = (8.5 \pm 2)$.

In a recent combined solubility and spectroscopic study [9], Cho and co-workers determined the solubility product of freshly precipitated $\text{Pu}(\text{OH})_3(\text{am})$ phase and re-evaluated the first hydrolysis constant of Pu(III). A blue $\text{Pu}(\text{OH})_3(\text{am})$ precipitate was obtained by coulometric titration of a Pu(III) stock solution. The pH was varied between $3.10 \leq -\log [\text{H}^+] \leq 6.44$ (spectroscopic experiments) and $6.29 \leq -\log [\text{H}^+] \leq 8.42$ (solubility experiments). Plutonium

was retained in the +III redox state electrochemically throughout the experiments. Solid phase characterization by XRD indicated the amorphous character of the solid phase used in the solubility experiments. Based on their UV-Vis measurements, the authors reported a greater value for the first hydrolysis constant of Pu(III) than the current selection in the NEA-TDB [5]. Although reporting solubility data mostly consistent with the previous solubility study by Felmy et al. [7], Cho and co-workers determined a significantly lower $\log^* K_{s,0}^{\circ}(\text{Pu}(\text{OH})_3(\text{am}))$ as a result of a different hydrolysis scheme considered in their calculations. The results presented in Cho et al. [9], suggest that $\text{Pu}(\text{OH})_3(\text{am})$ is stable within the stability field of water, and converts to $\text{PuO}_2(\text{am,hyd})$ only above $(\text{pe} + \text{pH}) = (0.8 \pm 0.5)$.

The reductive dissolution of $\text{PuO}_2(\text{am,hyd})$ was more frequently investigated [6, 10–12]. This is probably due to the relatively large co-existent stability field for $\text{PuO}_2(\text{am,hyd})$ and $\text{Pu}(\text{III})_{\text{aq}}$. All these studies were performed within the pH-range 4–9, and provided an accurate control of the redox conditions by using hydroquinone ($\text{C}_6\text{H}_6\text{O}_2$), $\text{Na}_2\text{S}_2\text{O}_4$ or Fe(0) powder. As a result of this experimental effort and due to the well-defined $(\text{pe} + \text{pH})$ conditions in these studies, the thermodynamic data available for the redox equilibrium $\text{Pu}(\text{IV})_{\text{s}} + \text{e}^- \rightleftharpoons \text{Pu}(\text{III})_{\text{aq}}$ from mildly acidic to mildly alkaline pH conditions can be considered to be rather accurate. However, similar investigations under alkaline to hyperalkaline conditions are missing so far, reflecting the challenge that the stability field of Pu(III) aqueous species is expected to be smaller. Indeed, the hydrolysis of Pu(III) was only investigated under acidic to near-neutral pH conditions where the first hydrolysis species (PuOH^{2+}) forms [13–15] (for further details see the critical review provided in the recent NEA-TDB update book [5]). Thermodynamic data for higher hydrolysis species of Pu(III) are normally estimated based on data for Am(III) and Cm(III) [5].

Both the solubility of Pu(III) and the reductive dissolution of Pu(IV) were comprehensively reviewed in Neck et al. [2]. Based on the reported experimental evidences and with special focus on $(\text{pe} + \text{pH})$ measurements, a satisfactory explanation of the experimental observations with the available thermodynamic data selection by NEA-TDB [5] was provided. Neck and co-workers also highlighted the relevant role that Pu(IV) colloids may play in the solubility and redox chemistry of Pu under near-neutral to alkaline pH conditions.

Fellhauer conducted a comprehensive study [16] on the redox chemistry of Pu under reducing conditions. Experiments were performed in 0.1 M NaCl systems at $3.3 \leq -\log [\text{H}^+] \leq 7.8$. The redox equilibria $\text{Pu}(\text{IV})_{\text{s}}/\text{Pu}(\text{III})_{\text{aq}}$

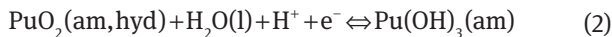
was evaluated over a broad range of $(\text{pe} + \text{pH})$ conditions using a large variety of redox buffers/chemicals (hydroquinone, $\text{FeCl}_2/\text{FeCl}_3$, $\text{Na}_2\text{S}_2\text{O}_4$, $\text{Fe}(\text{CN})_6^{4-}/\text{Fe}(\text{CN})_6^{3-}$ and Anthra(hydro)quinone-2,6,-disulfonate: $\text{AH}_2\text{QDS}/\text{AQDS}$). The author concluded that the abovementioned redox equilibrium can be properly described with the available thermodynamic data. However, based on the solubility and solid phase characterization data collected for one of the most reducing samples at $-\log [\text{H}^+] = 6.6$, Fellhauer concluded that the solubility of $\text{Pu}(\text{OH})_3(\text{am})$ reported in the work of Felmy et al. [7] might be significantly overestimated but still within the uncertainty range proposed by the NEA-TDB [5].

Besides solution chemistry studies in homogeneous systems, a number of experimental investigations have focussed on the redox chemistry of Pu in heterogeneous systems [16–23], in many cases involving interaction with Fe phases (particularly magnetite, Fe_3O_4). Most of these studies were performed under acidic to weakly alkaline pH conditions. Based on a combination of EXAFS and solution chemistry measurements (pH, pe and $[\text{Pu}]$), Kirsch et al. [19] reported a qualitative agreement between thermodynamic calculations and experimentally measured Pu redox distribution in magnetite, mackinawite (FeS) and chukanovite ($\text{Fe}_2(\text{CO}_3)(\text{OH})_2$) systems with $6 \leq -\log [\text{H}^+] \leq 8$. In the magnetite system, the authors observed the formation and predominance of a very stable Pu(III) surface complex, whereas $\text{PuO}_2(\text{am,hyd})$ prevailed in the presence of mackinawite and chukanovite. González-Siso et al. [23] also observed the stabilization of Pu(III) sorbed in magnetite under hyperalkaline ($-\log [\text{H}^+] = 12.8$) and very reducing conditions imposed by SnCl_2 ($\text{pe} + \text{pH} = 2 \pm 1$). Although the role of the Fe(II)–Fe(III) surface is expected to be relevant for the reduction of Pu in this system, this observation opens the possibility for Pu(III) stabilization under the hyperalkaline reducing conditions relevant to certain repository concepts.

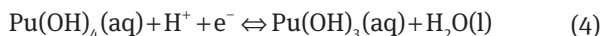
1.2 Thermodynamic background

Considering the alkaline to hyperalkaline pH conditions prevailing in cementitious systems ($10 \leq \text{pH} \leq 13.3$), the solid compounds $\text{Pu}(\text{IV})\text{O}_2(\text{am,hyd})$ and $\text{Pu}(\text{III})(\text{OH})_3(\text{am})$, as well as the aqueous species $\text{Pu}(\text{IV})(\text{OH})_4(\text{aq})$ and $\text{Pu}(\text{III})(\text{OH})_3(\text{aq})$ are expected to control the redox chemistry of Pu in the absence of any complexing ligand besides water/hydroxide. In view of the thermodynamic data selection provided in NEA-TDB [5] and Neck et al. [2], reactions (2), (4), (6), and corresponding stability constants

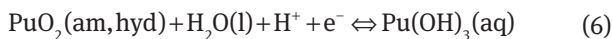
can be defined for the Pu redox equilibria in the solid, aqueous and mixed phases, respectively.



$$\log {}^*K_{\text{IVs/III s}}^{\circ} = \text{pH} + \text{pe} - \log a_{\text{w}} = -(0.4 \pm 1.6) \quad (3)$$



$$\log {}^*K_{\text{IVaq/IIIaq}}^{\circ} = \log a_{\text{Pu}(\text{OH})_3(\text{aq})} + \log a_{\text{w}} - \log a_{\text{Pu}(\text{OH})_4(\text{aq})} + \text{pH} + \text{pe} = (0.0 \pm 0.7) \quad (5)$$



$$\log {}^*K_{\text{IVs/IIIaq}}^{\circ} = \log a_{\text{Pu}(\text{OH})_3(\text{aq})} + \text{pH} + \text{pe} - \log a_{\text{w}} = -(10.8 \pm 0.7) \quad (7)$$

As indicated in the discussion above, the very large uncertainties associated to $\log {}^*K_{\text{IVs/III s}}^{\circ}$, $\log {}^*K_{\text{IVaq/IIIaq}}^{\circ}$ and $\log {}^*K_{\text{IVs/IIIaq}}^{\circ}$ difficult the assessment of Pu redox chemistry under hyperalkaline reducing conditions. These uncertainties further affect the evaluation of the impact of other inorganic/organic ligands on the solubility of Pu. In this framework, this work aims at characterizing the solid phase controlling the solubility of Pu under reducing alkaline conditions, to decrease the uncertainties affecting the redox chemistry of Pu under the boundary conditions, and thus to provide an adequate basis for studying the interaction of Pu with inorganic/organic ligands relevant in the context of L/ILW and SFR.

2 Experimental section

2.1 Chemicals

All solutions were prepared with ultra-pure water purified with a Milli-Q apparatus (Millipore, 18.2 M Ω , 22 \pm 2 $^{\circ}$ C) and purged for several hours with Ar before use. C₈H₁₇NO₃S (CHES; p.a.), diethyl-ether (C₄H₁₀O, p.a.), NaCl (p.a.), NaOH (Tritrisol), HCl (Tritrisol), hydroquinone (p.a.), xylene (isomeric mixture, p.a.) and toluene (p.a.) were obtained from Merck. C₄H₁₁NO₃–C₄H₁₁NO₃·HCl (TRIS–TRIS·HCl; p.a.) and SnCl₂ (p.a.) were purchased from Sigma–Aldrich. 1-phenyl-3-methyl-4-benzoyl-pyrazol-5-one (PMBP) and Di-(2-ethylhexyl)-phosphoric acid (HDEHP) were obtained from Fluka (purum). Carbonate impurities in fresh 1.0 M NaOH (Tritrisol) were quantified as (3 \pm 1) · 10^{–5} M using a Shimadzu TOC5000 equipment.

A well-defined Pu standard solution with an isotopic composition of 99.4 wt.% ²⁴²Pu, 0.58 wt.% ²³⁹Pu, 0.005 wt.% ²³⁸Pu and 0.005 wt.% ²⁴¹Pu was used for the

standard addition method described in Section 2.4.1. The use of the long-lived ²⁴²Pu isotope (t_{1/2} = 3.75 · 10⁵ a) avoids redox processes induced by radiolysis.

All solutions and samples were prepared, stored, and handled inside an inert gas (Ar) glovebox at T = (22 \pm 2) $^{\circ}$ C.

2.2 Measurements of pH and E_h

Combination pH–electrodes (type Orion Ross, Thermo Scientific), freshly calibrated against standard pH buffers (pH = 8–13, Merck) were used to determine the total free concentration of proton in molal units (pH_m = –log₁₀ m_{H⁺}). In aqueous solutions of ionic strength I \geq 0.1 mol · kg^{–1}, the measured pH value (pH_{exp}) is an operational apparent value related to m_{OH[–]} by pH_m = pH_{exp} + A_m (pH_c = pH_{exp} + A_c), where A_m is an empirical parameter including the activity coefficient of the proton (γ_{H^+}) and the liquid junction potential of the electrode for a given background electrolyte and salt concentration. The empirical A_m values for NaCl were taken from the literature [24]. In NaCl–NaOH solutions with m_{OH[–]} > 0.03 m, the H⁺ concentration was calculated from the given m_{OH[–]} and the conditional ion product of water (calculated with the SIT model and available parameters from NEA-TDB [5]).

The redox potential E_h (versus standard hydrogen electrode SHE) in the batches was determined with a combined Pt and Ag/AgCl reference electrode (Metrohm). The measured potentials were converted into E_h by correcting for the potential of the Ag/AgCl inner-reference electrode at 3 M KCl and T = 22 $^{\circ}$ C (+207 mV). E_h values were further converted to pe = –log a_{e[–]} according to equation (8):

$$E_{\text{h}} = -RT \ln(10) F^{-1} \log a_{\text{e}^-}, \quad (8)$$

where R is the ideal gas constant (8.31446 J · mol^{–1} · K^{–1}), F is the Faraday constant (96,485.33 C · mol^{–1}) and a_{e[–]} is the activity of the electron. E_h values were collected following the protocol described in Altmaier et al. [25], which involved approximately 15 min equilibration time. Very stable E_h readings were obtained in hydroquinone and in most of the SnCl₂ samples. Because of the low concentration of Sn(II) in the aqueous phase due to the precipitation of Sn(II) solid phases (SnO(cr) or Sn₆O₄(OH)₄(s), see Gamsjäger et al. [26]), E_h measurements in SnCl₂ samples with pH_m \leq 9 normally required longer equilibration times. For the latter systems, the absolute drift of the electrode was strictly < 0.5 mV/min. The uncertainty of the measured values was determined as 2 σ of repeated E_h readings and resulted in \pm 30 mV for all the samples stabilized with redox buffers, except for the SnCl₂ samples at pH_m \leq 9,

for which an uncertainty of ± 60 mV was obtained. The latter systems are characterized by the quantitative precipitation of SnO and consequent decrease of Sn(II) concentration in solution, which decreases the sensitivity of the measurement. The uncertainty of E_h measurements in systems without redox buffers is discussed in Sections 3.2.1 and 3.3.2.

The accuracy of the combined redox electrode was checked with commercial redox-buffer solutions (+220 mV, Schott Instruments). Note that the available buffers provide rather oxidizing E_h readings under acidic to near-neutral pH conditions, and thus may not be representative of the experimental conditions in this study (hyperalkaline and strongly reducing). A number of recent experimental studies [16, 23, 27] at KIT-INE using Pu(IV)/Pu(III), U(VI)/U(IV) and Tc(VII)/Tc(IV) as redox indicators in the presence of redox buffers (hydroquinone: HQ, SnCl₂, Fe(0), Na₂S₂O₄) have shown the reasonable agreement between measured E_h values and thermodynamic calculations under alkaline to hyperalkaline reducing conditions, with deviations from the reference (thermodynamic) value below 50 mV.

2.3 Pu solubility experiments

The solid phase PuO₂(am,hyd) used in this study was originally precipitated in 2006 and has been stored to date in aqueous solution under controlled Ar-atmosphere. The plutonium used for the preparation of the solid phase consisted of an isotopic composition of 99.4 wt.% ²⁴²Pu, 0.58 wt.% ²³⁹Pu, 0.005 wt.% ²³⁸Pu and 0.005 wt.% ²⁴¹Pu. The original solution was purified from the daughter nuclides and characterized by α -, γ -spectrometry and ICP-MS. The resulting Pu stock solution (in 1.0 M HClO₄, containing a mixture of different oxidation states) was quantitatively reduced on a platinum cathode at $E_{\text{cathode}} = -0.2$ V to Pu(III) followed by a partial oxidation to Pu(IV) at $E_{\text{anode}} = +0.8$ V. UV-vis/NIR spectroscopy indicated a Pu⁴⁺:Pu³⁺ ratio in the final solution of approximately 3:1. Slow addition of 0.1 M NaOH yielded a dark green precipitate of Pu(IV) hydrous oxide, which was washed several times with water and stored in 0.1 M NaCl for 2 weeks. The precipitate was then distributed to six samples in 0.1 M NaCl solutions with $3 \leq \text{pH}_m \leq 6$. Since the original preparation, the samples have been regularly monitored for pH_m , E_h and Pu concentration after 10 kD ultrafiltration. The last sampling of this series was accomplished in the context of the current study and corresponds to an equilibration time of 2886 days (79 years). The redox state distribution of Pu in selected samples of this series was determined using

a liquid-liquid extraction method previously described elsewhere [2], and a capillary electrophoresis hyphenated sector-field inductively coupled plasma mass spectrometry technique CE-SF-ICP-MS (see Sections 2.4.2 and 2.4.3, respectively).

Two series of batch experiments (with total volumes of 25 mL) were prepared differing in the redox conditions, which were either buffered by 2 mM hydroquinone or SnCl₂. The former defines mildly reducing conditions ($\text{pe} + \text{pH}_m \approx 10$) where Pu(IV) is the only oxidation state of Pu in the system. Strongly reducing redox potentials close to the border of water reduction were adjusted with SnCl₂ ($\text{pe} + \text{pH}_m \approx 2$), in accordance with previous studies [27, 28]. Owing to the large uncertainties in thermodynamic data available for Pu aqueous species and compounds forming in these alkaline and very reducing conditions, both Pu(III)_{s/aq} and Pu(IV)_{s/aq} might be stable (relevant) in the samples buffered with SnCl₂.

Ionic strength was maintained constant in all the samples with 0.1 M NaCl-NaOH solutions. In both series (hydroquinone and SnCl₂), pH_m values of the matrix solutions were adjusted between 8 and 13. Systems at $\text{pH}_m = 8$ and 9 were buffered with 20 mM of TRIS and CHES, respectively. Whenever necessary, pH_m was adjusted with HCl and NaOH solutions of same ionic strength. After achieving constant readings of pH_m and E_h values (within the related given uncertainties), PuO₂(am,hyd) solid phase was added to the system.

The aged Pu solid phase (≈ 8 years) at $\text{pH}_m = 5.93$ was newly characterized for this study using powder X-ray diffraction (XRD), X-ray Photoelectron Spectroscopy (XPS), X-ray absorption near edge spectroscopy (XANES) and extended X-ray absorption fine structure spectroscopy (EXAFS) (see Section 2.5). Approximately 0.2 mg of this solid phase were added to each of the batches. A larger amount (*ca.* 1 mg) was added to four selected samples with $\text{pH}_m = 9$ and 12 (of both hydroquinone and SnCl₂ systems) aiming at a later solid phase characterization.

After the addition of the solid phase, pH_m , E_h and m_{Pu} of all the samples were regularly monitored. The aqueous concentration of Pu was measured after phase separation by 10 kD ultrafiltration (pore size ≈ 2 nm) (Nanosep®, Pall Life Sciences) using liquid scintillation counting (LSC, see Section 2.4.1). The concentration of Pu in the supernatant was also measured by LSC without any phase separation with the purpose of assessing the presence of Pu(IV) intrinsic colloids. For specific samples in the alkaline to hyperalkaline pH-region, phase separation was also performed by ultra-centrifugation at 90,000 rpm (694,000 g) (Beckman XL-90, rotor type 90Ti) in welded vials for 1 h. Ultra-centrifugation is able to remove Pu(IV) intrinsic

colloids, whilst avoiding the potential sorption of Pu on the 10 kD filters. After centrifugation, an aliquot of the supernatant was acidified with 2% HNO₃ and Pu concentration was determined by either standard or inductively coupled plasma-sector field mass spectrometry (ICP–MS PerkinElmer ELAN 6100 and SF–ICP–MS Thermo Element XR, respectively). The detection limits of these techniques for Pu in the conditions of this study are approximately $\sim 10^{-10.5}$ M and $\sim 10^{-12}$ M, respectively. Depending upon dilution factor and total concentration of Pu, standard deviations in (SF–)ICP–MS measurements varied from 5 to 60%. Plutonium concentrations measured in molar units (M) were converted to the molal scale (m, mol · kg_w⁻¹) using the conversion factors reported for NaCl solutions in the NEA-TDB [5].

Equilibrium conditions were assumed after repeated measurements with constant pH_m, E_h and total plutonium concentration (m_{Pu}), and were normally achieved within 30 days. No trend of m_{Pu} with time was observed after this equilibration period. After attaining equilibrium conditions, the selected solid phases from the solubility series in hydroquinone and SnCl₂ were characterized by XPS, XAFS and *in-situ* XRD as described in Section 2.5.

2.4 Characterization of the aqueous phase

2.4.1 Liquid scintillation counting of ²⁴²Pu

Liquid scintillation counting (LSC) was used for the quantification of m_{Pu} in those samples with greater solubility (mostly under acidic conditions). The isotopic composition of Pu stock solution and solid phases used in this study includes α-(²⁴²Pu, ²³⁹Pu, ²³⁸Pu) and β-(²⁴¹Pu) emitters, as well as traces of the α-emitter ²⁴¹Am resulting from the decay of ²⁴¹Pu (t_{1/2} = 14.35 a). Due to the very close energy of the α-peaks of ²⁴²Pu, ²³⁹Pu, ²³⁸Pu and ²⁴¹Am and the uncertainty associated to the contribution of ²⁴¹Am to the total counts, the concentration of Pu in solution was quantified using the signal of the low-energetic β-emitter ²⁴¹Pu.

Aliquots of the untreated supernatant (including potential colloidal fractions) and of the 10 kD ultrafiltered sample were acidified with 2% HNO₃ and mixed with 10 mL of LSC cocktail (Ultima Gold XR, Perkin Elmer). LSC measurements were performed on a low-level LSC equipment type Quantulus 1220 (LKB WallacOy, now PerkinElmer) for 30 min. Standard addition with 50 μL of well-defined Pu stock solutions (4.36 · 10⁻⁷ M or 3.18 · 10⁻⁷ M) with the same isotopic composition was used to account for the potential quenching effect of the matrix solution on the counting efficiency of ²⁴¹Pu of unknown samples. Standard

deviation for independently measured concentrations of a sample was found to be approximately 10–30%, depending upon dilution factor and total Pu concentration.

The detection limit of the LSC technique under the conditions of this study is about $\sim 10^{-9.2}$ M, clearly above the expected solubility of PuO₂(am,hyd) under alkaline pH conditions. Thus, the quantification of Pu concentration in most of the samples was also performed using ICP–MS and SF–ICP–MS techniques with detection limits of $\sim 10^{-10.5}$ M and $\sim 10^{-12}$ M, respectively.

2.4.2 Liquid-liquid extraction

The oxidation state of Pu in the aqueous phase was determined for selected samples using the liquid-liquid extraction method described in Neck et al. [2]. The method is a combination of previously reported approaches [29–33], and allows the quantification of Pu(III), Pu(IV), Pu(V), Pu(VI) and colloidal Pu(IV) with an uncertainty of 20% (for the Pu concentration-range evaluated in this study). Note further that the reliability of the method is greater for the separation/identification of the groups (Pu(III) + Pu(IV)) and (Pu(V) + Pu(VI)), because of the slower redox transformation kinetics of Puⁿ⁺ ↔ PuO₂^{z+}.

The extraction was performed after 10 kD ultrafiltration for those samples with m_{Pu} ≥ 10⁻⁷ m (acidic series, pH_m = 3.76, 3.86). Before contacting the aqueous solution with the organic phase, an aliquot (375 μL) of the filtered sample was acidified to pH = 0 with 375 μL of HCl 2.0 M. 1-phenyl-3-methyl-4-benzoyl-pyrazol-5-one (PMBP) dissolved in xylene and Di-(2-ethylhexyl)phosphoric acid (HDEHP) dissolved in toluene were used as extractants for Pu(IV) and (Pu(IV) + Pu(VI)), respectively. The combination of both extraction steps with an additional rapid oxidation step (using K₂Cr₂O₇) of Pu(III) to Pu(IV) and Pu(V) to Pu(VI) provides the complete redox state distribution of Pu in the aqueous phase (see Table 1).

After the separation of the aqueous and organic phases, both aliquots were added to 10 mL of LSC cocktail and the Pu concentration was determined by LSC. The same extraction procedure was carried out with MilliQ water to correct for the contribution of changes in the background electrolyte solutions in the LSC measurements.

2.4.3 CE-SF–ICP–MS

The oxidation state distribution of Pu was also investigated by capillary electrophoresis hyphenated to inductively coupled plasma-sector field mass spectrometry

Table 1: Distribution of Pu oxidation states in the organic and aqueous phases according to the extraction method used in this work.

Method	Oxidation state distribution	
	Organic phase	Aqueous phase
PMBP extraction at pH=0	Pu(IV)	Pu(III), (IV)coll ^a , (V), (VI)
PMBP extraction at pH=0, with K ₂ Cr ₂ O ₇	Pu(III), (IV)	Pu(IV)coll ^a , (V), (VI)
HDEHP extraction at pH=0	Pu(IV), (VI)	Pu(III), (IV)coll ^a , (V)
HDEHP extraction at pH=0, with K ₂ Cr ₂ O ₇	Pu(III), (IV), (V), (VI)	Pu(IV)coll ^a

^aPu(IV)coll refers to the colloidal species of Pu(IV).

(CE–SF–ICP–MS). All separations were carried out with a commercial Beckman Coulter P/ACE MDQ capillary electrophoresis system. The hyphenation of the CE to the SF–ICP–MS (Thermo Element XR) instrument was achieved using a Mira Mist CE nebulizer (Burgener Research, Mississauga, ON, Canada). A conventional fused-silica capillary with 75 µm internal diameter and 73 cm length was used for separation. Before the first use, each capillary was conditioned with 0.1 M HCl (Merck, Suprapur), 0.1 M NaOH (Merck, Titripur), Milli-Q water and 1.00 M acetic acid (background electrolyte, BGE) for several hours. The temperature of the capillary was kept constant at $T=15\text{ }^{\circ}\text{C}$ during the separation. Under the given experimental conditions, the temperature gradient across the capillary's cross section was estimated to be $0.7\text{ }^{\circ}\text{C}$.

The capillary was washed with the BGE for 5 min at 20 psi before each measurement. Separations were performed with +30 kV applied potential at a constant pressure of 0.4 psi and accomplished within 20 min. The rinsing sequence after each separation included 0.1 M HCl, 0.1 M NaOH and BGE. Sample injection (approximately 2.3 nL) was performed hydrodynamically at 2 psi for 10 s. The CE equipment was placed in a N₂ glovebox (O₂ < 5 ppm) to avoid any alteration in the redox state of Pu. A more detailed description of the method is given in Graser et al. [34].

2.5 Characterization of the solid phase

2.5.1 XRD

Approximately 0.5 mg of the equilibrated solid phase were taken from selected solubility samples and washed four times with ethanol under Ar–atmosphere to remove the traces of background electrolyte (NaCl). The resulting solid was re-suspended with 25 µL ethanol, placed on a single crystal silicon waver and dried up at room temperature under Ar atmosphere. Powder X-ray diffraction (XRD) measurements were performed using a D8 Advance

diffractometer (Bruker AXS, Germany) equipped with a Cu radiation tube (Cu K– α , $\lambda=0.15418\text{ nm}$, current: 25 mA, voltage: 40 kV), Ni filter and a Sol–X detector. The XRD pattern was recorded in the range of $5^{\circ}\leq 2\theta\leq 80^{\circ}$ with a step size of 0.015° and a counting time of 6 seconds per step. Data were processed using the Bruker AXS Diffrac-Plus EVA software (Bruker AXS, Germany, version 3.1). The resulting diffractograms were compared to the XRD patterns of possibly relevant solid phases available in the JCPDS database [35]. Rietveld refinement was performed with the Bruker DiffracPlus TOPAS software package (Bruker AXS, Germany, version 4.2).

2.5.2 XAFS and (synchrotron-based) *in-situ* XRD

X-ray Absorption Fine Structure (XAFS) spectra and Laue-type *in-situ* diffractograms were recorded at the INE–Beamline [36] for Actinide Research at ANKA, KIT Campus Nord. The ANKA storage ring was operated at 2.5 GeV electron energy with a mean electron current of 120 mA. The set-up available at the INE–Beamline for the *in-situ* XRD characterization of active samples is a unique, non-invasive tool for the investigation of redox-sensitive solid phases.

The tuneable monochromatic beam was delivered by a double crystal monochromator (DCM), equipped with a pair of Ge(422) crystals ($2d=2.310\text{ \AA}$). Possible higher harmonic radiation was suppressed by detuning the parallel alignment of the crystals to obtain 70 % of photon flux peak intensity at the rocking curve maximum.

All samples for XAFS and (synchrotron-based) *in-situ* XRD measurements were prepared in 400 µL polyethylene vials. A suspension containing $\approx 1\text{ mg}$ of material was transferred to the vial and centrifuged for 10 min at 4020 g. The vial was heat sealed in a plastic bag (polyethylene), mounted in a gas-tight cell inside the Ar–glovebox and transported to the INE–Beamline. During the XAFS measurements, Ar was continuously flushed through the cell to ensure inert atmosphere. Data collection was performed at $T=(22\pm 2)\text{ }^{\circ}\text{C}$.

XANES spectra of the Pu L_{III} -edge (E ($2p_{3/2}$) Pu(0): 18,057 eV) were recorded in fluorescence yield detection mode using a 5-pixel low energy Ge solid-state fluorescence detector (C Canberra-Packard Ultra-LEGe, Olen, Belgium) and an Ar-filled ionization chamber at ambient pressure to record the incident beam intensity. 8–10 scans were collected for each Pu sample. The spectra were calibrated against the first inflection point in the K-edge spectrum of a Zr metal foil (E (1s) Zr(0): 17,998 eV) and averaged to reduce statistical noise. XANES and EXAFS data reduction were performed with the ATHENA program package [37], following standard procedures for edge jump normalization and EXAFS $\chi(k)$ extraction. E_0 , the origin for calculating the EXAFS $\chi(k)$ -function, was fixed at the ‘white line’ (WL) peak maximum in the XAFS spectra at $\approx 18,068$ eV. The Pu L_{III} -edge XANES spectra obtained in this work were compared with previously reported [38, 39] Pu(III) and Pu(IV) reference spectra collected at the INE-Beamline under the same experimental conditions and data analysis procedure. A linear combination exercise was performed using the Pu(III)_{aq} and Pu(IV)_{aq} reference spectra described above as main components. The fit was conducted using ATHENA program package [37], and allowed the quantification of the fraction of Pu(III) and Pu(IV) in the samples investigated in the present work. Uncertainties were obtained as standard deviations of the minimization approach embedded within the software.

EXAFS data analysis was based on standard least squares fit techniques using the UWXAFS program package [40]. Metric parameters (i. e. neighbor atom distances R_i , EXAFS Debye-Waller factors σ_i^2 , coordination numbers N_i for the different coordination shells i) were determined using the feffit code (v2.98). Backscattering amplitude and phase shift functions for single scattering paths in a 45-atom PuO₂ cluster with fluorite structure were obtained from FEFF8.2 calculations [41]. All fit operations were performed in R-space over the individual radial distance ranges given in Table 3. The amplitude reduction factor S_0^2 was fixed at 1.0.

After completing the XAFS data accumulations, the samples were individually taken out of the Ar-flushed sample cell, and the *in-situ* diffractograms were collected. The double containment (vial and an outer plastic bag) in addition to the redox buffers in the protecting solution (hydroquinone and SnCl₂) underneath the Ar atmosphere are considered to be sufficient to avoid any redox transformation of the bulk material within the timeframe of the XRD measurements (approximately 5–10 min).

The 2D XRD patterns were recorded in Laue transmission geometry using radiation sensitive high efficiency storage phosphor screens (V×H: 125 mm×252 mm) with

a high dynamic range (MultiSensitive Phosphor Screen, PerkinElmer, Germany). The screen was mounted perpendicular to the incident beam (E=17.0 keV, $\lambda_{exc} = 0.7$ Å, size (V×H) 200 μm×500 μm) at a distance of 20 cm from the sample. An indium metal disk, mounted on the tip of a plastic rod was used as central beam-stop. The irradiated phosphor screen was scanned by a laser based read-out system (Cyclone Plus Phosphor Imager, PerkinElmer LAS, Rodgau-Jügesheim, Germany), transforming the diffracted 2D X-ray intensity into a high resolution digitized image (600 dpi) with quantitative data as an image file (OptiQuant™ software).

The collected frames were transformed into one-dimensional diffraction patterns by using the XRDU software package [42]. The images were corrected for dark-current, spatial distortion and detector pixel response. The XRD pattern of an Y₂O₃ powder sample was used as reference for calibration [43]. After correcting and calibrating the images, azimuthal integration was performed and the resulting diffractograms were normalized for the incident beam intensity. The background subtraction was achieved with a cubic spline polynomial fitting of the baseline.

2.5.3 XPS

A few μL of a suspension containing Pu solid phase from selected solubility experiments were placed on an indium foil and subsequently dried under Ar-atmosphere. A vacuum transfer vessel was used to move the samples mounted on a sample holder into the inlet of the XPS without air contact. The X-ray photoelectron spectrometer (ULVAC-PHI, Inc., model PHI 5000 VersaProbe II) is equipped with a scanning microprobe X-ray source (monochromatic Al Kα, 1486.6 eV). Surface charge compensation of analysed sample areas was achieved by combination of an electron flood gun and a floating ion gun generating low energy electrons (1 eV) and low energy Ar ions (6 eV) (dual beam technique), respectively. Calibration of the binding energy scale of the spectrometer was performed using well-established [44] binding energies of elemental lines of pure metals (monochromatic Al Kα: Cu $2p_{3/2}$ at 932.62 eV, Au $4f_{7/2}$ at 83.96 eV). Survey scans were recorded with a source power of 31 W of the scanning microprobe X-ray source, beam diameter 200 μm, and pass energy of 187.85 eV of the analyser to identify the elements present. To retrieve information about the chemical state of the elements, narrow scan spectra of elemental lines were recorded at pass energy of 23.5 eV, step size 0.1 eV. Data analysis was performed using PHI MultiPak program, version 9.6.0.

3 Results and discussion

3.1 Characterization of the PuO₂(ncr,hyd) starting material

After preparation (cf. Section 2.3), PuO₂(ncr,hyd) was aged for ~ 8 years in a 0.1 M NaCl solution with pH_m ~ 6. In the subsequent discussion and figures this solid phase is referred as the “starting Pu material”. The long pre-equilibration time of the solid ensures that solubility experiments are not impacted by short-term alterations of the solid phase, e. g. by changes in crystallinity, and hence solubility.

The XRD pattern of the starting Pu material perfectly matches the reference pattern of PuO₂(cr) corresponding to the file 41-1170 in the JCPDS database [35] (Figure 4 in Section 3.2.3). The peak widths in the diffractogram are consistent with a nanocrystalline structure. Rietveld refinement (on Fm $\bar{3}$ m space group) of the collected pattern revealed a mean value of the crystal domain size of (4 ± 1) nm and an average cell parameter of (5.405 ± 0.005) Å. This is in good agreement with the reference value reported in the literature [45, 46] (5.396 Å).

The white line energy position in the Pu L_{III} XANES spectrum of the starting Pu material is in excellent agreement with the Pu(IV) reference spectrum reported in Brendebach et al. [38] (Figure 5 in Section 3.2.3). Differences in amplitude observed between both spectra are related with the state of Pu in the sample (solid in the present work, aqueous in the reference [38]), as previously discussed in Rothe et al. [47]. The EXAFS fit parameters obtained for this sample (cf. Table 3) are in good agreement with those obtained for Pu(IV)(OH)₄(am)¹ precipitate in reference [48] [i. e. 4.3 (4.0) oxygen atoms at R_{Pu-O} = 2.33 (2.32) Å and 2.3 (2.4) plutonium atoms at R_{Pu-Pu} = 3.84 (3.87) Å]. The apparently low coordination numbers for both next neighbor shells reflect the strongly distorted Pu coordination in these materials with different Pu to -O²⁻, -OH₂, -OH⁻ distances and a high density of voids and dislocations, while this phase is still sufficiently ordered to exhibit a regular Pu-Pu second next neighbor interaction. Note that the fit significantly worsens when fixing the first shell coordination number to 8 (cf. Table 3 and the discussion in Section 3.2.3).

The X-ray photoelectron spectrum of the starting Pu material is also in accordance with the findings of XRD and

XANES measurements. Pu 4f photoemission peak exhibit a spin-orbit doublet for the Pu 4f_{7/2} peak at about 426.2 eV, in line with previously reported values [49–51]. A satellite is observed at approximately 6.9 eV higher binding energy than the Pu 4f main line. The difference in energy between the main line and the satellite is in agreement with data previously reported [49] for PuO₂(cr).

All experimental evidences collected for the starting Pu material (XRD, XANES, EXAFS, XPS) are consistent with the predominance of PuO₂(ncr,hyd). This solid phase is therefore established as the anchor point in the interpretation of the solubility data obtained under alkaline to hyperalkaline pH conditions.

3.2 Solubility experiments

3.2.1 pH and E_h measurements

The experimentally measured pH_m and E_h (converted into pe) values of all the evaluated samples are shown in the Pourbaix diagram of Pu in Figure 1. Thermodynamic solubility and hydrolysis constants for plutonium reported in Neck et al. [2] were used in the calculations. SIT ion interaction parameters estimated in the work of Neck and Kim [52] were used to account for ionic strength corrections of Pu(IV), whereas ε(i,j) values reported elsewhere [53] for Am(III) and Nd(III) were taken by analogy for the corrections of Pu(III) aqueous species. The ε(i,j) values reported in Gaona et al. [54] for Np(VI) were taken for the SIT corrections of the analogous Pu species.

Experimentally measured pH_m and E_h values for redox unbuffered samples (prepared previously to this study, see Section 2.3) under acidic conditions (symbols ● and ○ in Figure 1) scatter around the redox neutral line at (pe + pH_m) = 13.8. These measured E_h values are considered less reliable due to the low concentration of plutonium in solution (below 10⁻⁵ M, see also Figure 2), which is considered to control the redox potential in the absence of other redox couples in the system.

Pu solubility samples in the presence of hydroquinone and SnCl₂ showed stable pH_m (± 0.05) and E_h (± 30 – 50 mV, depending upon pH-region) values over the time frame (~ 9 months) of the solubility experiment (Figure 1). Hydroquinone sets moderately reducing conditions with (pe + pH_m) = (9.5 ± 1), which clearly are situated in the stability field of Pu(IV)_s and Pu(IV)_{aq}. This system is therefore considered as the reference Pu(IV) case in the present study. Tin(II) is a strong reducing agent which buffers the redox potential at (pe + pH_m) = (2 ± 1), i. e. very close to the border of water reduction. Under these conditions,

¹ The notation Pu(IV)(OH)₄(am) corresponds to a freshly precipitated Pu(IV) amorphous phase. Both Pu(IV)(OH)₄(am) and Pu(IV)O₂(am,hyd) are considered in the NEA-TDB reviews for amorphous, hydrous Pu(IV) oxides. The latter is nevertheless preferred, and has been also adopted in the present work.

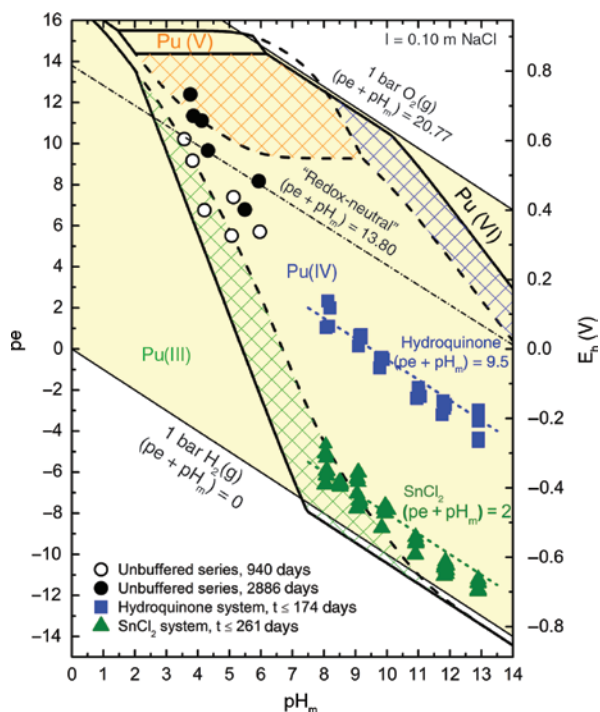


Figure 1: Pourbaix diagram of Pu calculated for $m_{\text{Pu}} = 10^{-5}$ m and $I = 0.10$ m NaCl using thermodynamic and (SIT) activity models described in the text.

pH_m and E_h values experimentally determined for Pu(IV) solubility experiments in the absence of redox buffers (O: 940 days, ●: 2886 days), and in the presence of hydroquinone (■) and SnCl_2 (▲). Thick lines correspond to redox borderlines between Pu(IV) and other Pu redox states: solid line is the borderline between Pu solid phases; dashed line is the borderline between Pu aqueous species. Colored regions indicate equilibrium between Pu(IV)_s and $\text{Pu(III)}_{\text{aq}}$ (green), Pu(V)_{aq} (orange) and $\text{Pu(VI)}_{\text{aq}}$ (blue). The borderlines of the stability field of water at $(\text{pe} + \text{pH}_m) = 20.77$ and $(\text{pe} + \text{pH}_m) = 0$, the “redox-neutral” line at $(\text{pe} + \text{pH}_m) = 13.8$ and the lines at $(\text{pe} + \text{pH}_m) = 2$ and 9.5 are shown for comparison.

currently available thermodynamic data [5] predict the predominance of Pu(IV) both in the aqueous and solid phases at $\text{pH}_m > 9$. Below this pH_m , the predominance of Pu(III) hydroxo-species (with the consequent increase of solubility due to the reductive dissolution of $\text{PuO}_2(\text{am,hyd})$) is expected (see Figure 1). As discussed in Section 1.3, the uncertainty affecting the thermodynamic data available for the redox equilibria controlling the solution chemistry of Pu under these conditions results in an ill-defined Pu(IV)/Pu(III) redox border, especially at $\text{pH}_m > 9$.

3.2.2 Solubility measurements

Total concentrations of plutonium in equilibrium with $\text{PuO}_2(\text{ncr,hyd})$ in the absence and presence of redox

buffers (hydroquinone, SnCl_2) are shown in Figure 2. The figure also shows the thermodynamically calculated solubility of $\text{PuO}_2(\text{am,hyd})$ in equilibrium with $\text{Pu(IV)}_{\text{aq}}$ species and for $(\text{pe} + \text{pH}_m) = 2$ (SnCl_2 system, both Pu(IV) and Pu(III) aqueous species contributing to solubility). Although not expected according to the Pourbaix diagram of Pu in Figure 1, Figure 2 includes also the thermodynamically calculated solubility of $\text{Pu(OH)}_3(\text{am})$ in equilibrium with $\text{Pu(III)}_{\text{aq}}$ species.

3.2.2.1 Acidic pH region, unbuffered systems

The measured solubility data for $\text{PuO}_2(\text{ncr,hyd})$ at $3.8 \leq \text{pH}_m \leq 6$ in unbuffered redox systems after an equilibration time of 940 (O) and 2886 (●) days are displayed in Figure 2. Data sets at $t = 940$ and 2886 days show consistent solubility values, indicating that thermodynamic equilibrium has been attained. The measured total concentrations of Pu are higher (more than 2 orders of magnitude) than calculated ones assuming equilibrium of $\text{PuO}_2(\text{am,hyd}) \rightleftharpoons \text{Pu(IV)}_{\text{aq}}$, with the available thermodynamic data selection [5] (see black solid line in Figure 2). On the other hand, Pu concentrations measured in these samples are clearly below the solubility of $\text{PuO}_{2+x}(\text{s,hyd})$ reported in Neck et al. [2].

To assess the potential contribution of other redox states of Pu to the total $\text{PuO}_2(\text{ncr,hyd})$ solubility under acidic conditions, liquid-liquid extraction and CE-SF-ICP-MS measurements were performed with the redox-unbuffered samples at $\text{pH}_m = 3.76$ and 3.86 . Liquid-liquid extraction showed the predominance of Pu(V) in both samples ($\geq 98\%$ of the total Pu concentration). In addition, lower contributions of Pu(VI) ($\log m_{\text{Pu}} = -7.3$ and -7.9 , respectively) and Pu(IV) concentrations ($\log m_{\text{Pu}} = -8.0$ and -8.3 , respectively) were determined (Figure 2). Even though the solvent extraction method is associated with large uncertainties notably for those redox states of low abundancies, the quantification of Pu(IV) is always more precise because the first step in the extraction scheme includes its selective extraction to the organic phase with PMBP (see Table 1 and in Nitsche et al. [30]). The quantification of $m_{\text{Pu(IV)}}$ by liquid-liquid extraction allows also the direct assessment of the equilibrium $\text{PuO}_2(\text{ncr,hyd}) \rightleftharpoons \text{Pu(IV)}_{\text{aq}}$ independently of the contributions of Pu(V) and Pu(VI). Although $m_{\text{Pu(IV)}}$ depicted in Figure 2 show already an excellent agreement with thermodynamic calculations for this equilibrium reaction, the results of the liquid-liquid extraction were used in combination with the hydrolysis scheme and corresponding equilibrium constants reported in NEA-TDB [5] to determine the

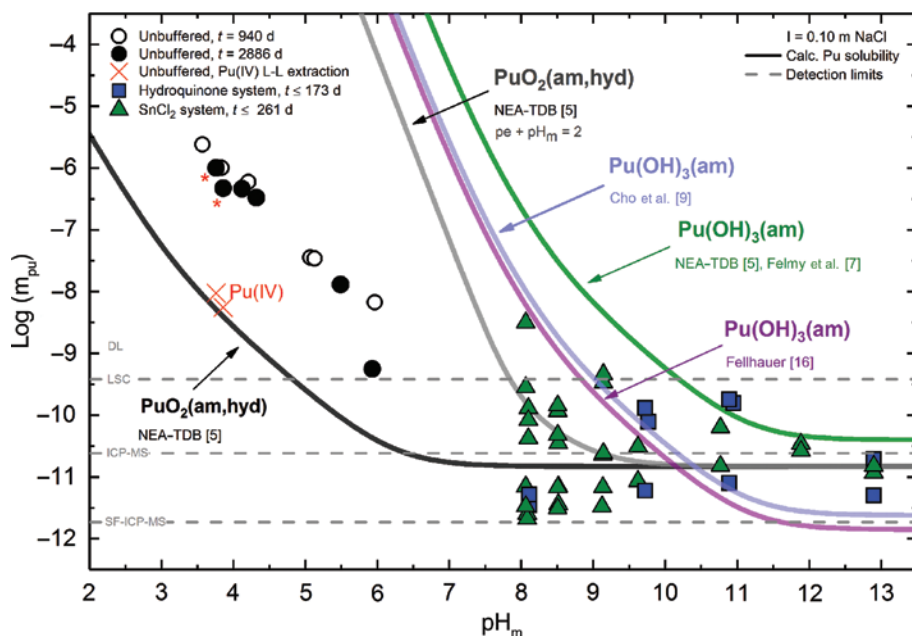


Figure 2: Plutonium total concentration in solution at $I = 0.10$ m NaCl in equilibrium with $\text{PuO}_2(\text{ncr,hyd})$ for redox unbuffered (O: 940 days, ●: 2886 days) and redox buffered systems (■: hydroquinone; ▲: SnCl_2). Red crosses (X) show the concentration of $\text{Pu(IV)}_{\text{aq}}$ for selected unbuffered systems (*) as quantified by liquid-liquid extraction. Solid lines correspond to the thermodynamically calculated solubility of $\text{PuO}_2(\text{am,hyd})$ in equilibrium with $\text{Pu(IV)}_{\text{aq}}$ (black line) and for $(pe + pH_m) = 2$ (gray line, predominance of $\text{Pu(III)}_{\text{aq}}$ at $pH_m \leq 9$). Green, purple and light blue lines show the solubility lines of $\text{Pu(OH)}_3(\text{am})$ as calculated with $\log {}^*K_{\text{III},0}$ values selected in the NEA-TDB [5] and reported in Fellhauer's work [16] and in Cho et al. [9], respectively. Horizontal dashed lines indicate the lowest limits of Pu quantification in solution for LSC, ICP-MS and SF-ICP-MS techniques, respectively.

$\log {}^*K_{\text{s},0}$ of the solid phase $\text{PuO}_2(\text{ncr,hyd})$ used in the present study (Section 3.3.1).

In order to crosscheck the results obtained by the solvent extraction method, the redox speciation determined by liquid-liquid extraction was analysed

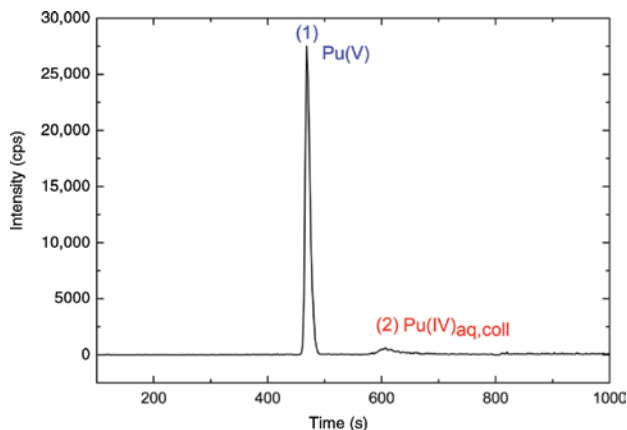


Figure 3: Electropherogram of the supernatant solution from the unbuffered Pu solubility experiment at $pH_m = 3.76$. Peak (1) is assigned to Pu(V)_{aq} , whereas peak (2) and characteristic tailing at $t > 600$ s corresponds to $\text{Pu(IV)}_{\text{aq}}$ and $\text{Pu(IV)}_{\text{coll}}$ species, respectively.

by CE-SF-ICP-MS. Figure 3 shows the electropherogram of the supernatant of the unbuffered sample with $pH_m = 3.76$. The first intense peak at $t \approx 470$ s with an electrophoretic mobility (μ) of $1.6 \cdot 10^{-4} \text{ cm}^2 \cdot \text{V}^{-1} \cdot \text{s}^{-1}$ is assigned to Pu(V)_{aq} as reported elsewhere [34]. The second peak at $t \approx 600$ s with $\mu = 1.2 \cdot 10^{-4} \text{ cm}^2 \cdot \text{V}^{-1} \cdot \text{s}^{-1}$ followed by a tailing at $t > 600$ s corresponds to Pu(IV) aqueous monomeric and polynuclear (colloidal) species [34]. The analysis clearly confirms the presence of Pu(IV) in the solution in agreement with the results obtained by applying the solvent extraction scheme. Pu(VI) , however, could not be identified. No signal above the detection limit of the method ($\sim 10^{-12}$ mol/L) was found suggesting a Pu(VI) species with an electric mobility of $\mu = 2.4 \cdot 10^{-4} \text{ cm}^2 \cdot \text{V}^{-1} \cdot \text{s}^{-1}$. This is consistent with the Pourbaix diagram in Figure 1, showing that the formation of Pu(VI) would only be expected at significantly higher pe conditions.

The predominance of Pu(V) in the aqueous phase confirmed by liquid-liquid extraction and CE-SF-ICP-MS is thus responsible for the enhanced solubility of $\text{PuO}_2(\text{ncr,hyd})$, and reflects the complexity of the redox chemistry of Pu. This is especially true in acidic conditions, where the predominance fields of Pu(III) , Pu(IV) and Pu(V) are close to each other (see Figure 1).

3.2.2.2 Alkaline to hyperalkaline pH region and reducing conditions

In this pH region, total concentration of Pu in equilibrium with $\text{PuO}_2(\text{ncr,hyd})$ measured by LSC after 10 kD ultrafiltration remains below or close to the detection limit of the technique ($10^{-9.2}$ m) for both the hydroquinone and SnCl_2 system.

Pu solubility data quantified by ICP-MS and SF-ICP-MS after ultracentrifugation are shown in Figure 2 for hydroquinone (■) and SnCl_2 (▲) systems (equilibration time: $t \leq 173$ and $t \leq 261$ days, respectively). Above $\text{pH}_m \approx 9$, very low concentrations of Pu ($10^{-9.9} \leq m_{\text{Pu}} \leq 10^{-11.4}$) are measured for both redox systems. Very low Pu concentrations are also measured at $\text{pH}_m = 8$ in the presence of hydroquinone, whereas m_{Pu} values with large uncertainties are obtained in the case of SnCl_2 . Significantly higher Pu concentrations ($m_{\text{Pu}} \approx 10^{-7.5} - 10^{-9}$ m) are obtained in the supernatant solutions in the absence of phase separation, both in hydroquinone and in SnCl_2 systems. This observation is consistent with the presence of Pu(IV) intrinsic colloids, as previously reported in the literature [2].

In spite of the scatter in the measured m_{Pu} ($\approx 1.5 \log_{10}$ -units) caused by the very low concentration of Pu and the predominance of neutral species in solution, data collected for the hydroquinone system are in agreement with the solubility expected for $\text{PuO}_2(\text{am,hyd})$ in equilibrium with Pu(IV) aqueous species (black solid line in Figure 2). A more complex picture arises in the case of SnCl_2 systems, where both the reductive dissolution of $\text{PuO}_2(\text{am,hyd})$ (gray line in Figure 2) and the solubility equilibrium $\text{Pu}(\text{OH})_3(\text{am}) \rightleftharpoons \text{Pu}(\text{III})_{\text{aq}}$ (green [5, 7], purple [16] and light blue [9] lines in Figure 2) would explain the experimental observations obtained in this study. A more detailed discussion in combination with the results obtained by *in-situ* XRD, XANES, EXAFS and XPS is provided in Section 3.3.2.

CE-SF-ICP-MS measurements were also performed for selected supernatant solutions of the Sn(II)-buffered system. In all cases, the only feature observed was an unusually elongated tailing of the electrophoretic peak of Pu(IV) aqueous species at $t > 600$ s, characteristic of the Pu(IV) colloidal species. These results, however, do not provide a definitive insight on the redox state of the Pu monomeric species prevailing in solution. It is worth mentioning that Pu(IV) intrinsic colloids have been previously proposed [2] to play a key role in the redox chemistry of Pu.

3.2.3 Solid phase characterization

3.2.3.1 Synchrotron-based *in-situ* XRD

Figure 4 shows the *in-situ* XRD patterns of the solid phases controlling the solubility of Pu in hydroquinone and SnCl_2

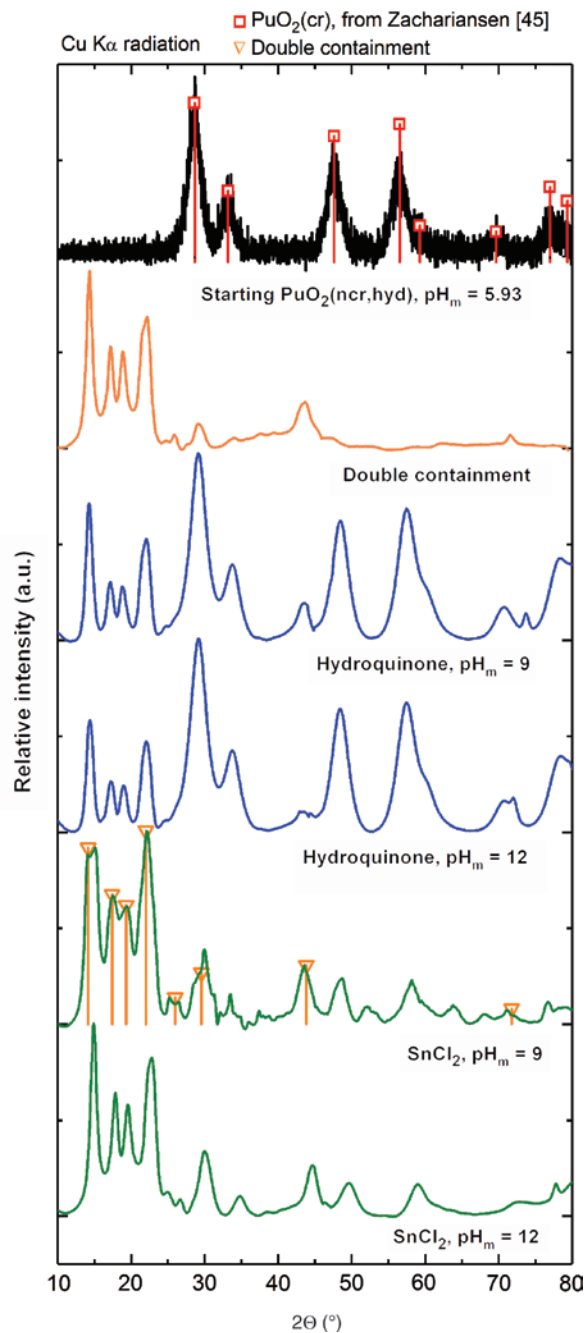


Figure 4: Powder diffractogram of the starting $\text{PuO}_2(\text{ncr,hyd})$ phase collected with a conventional spectrometer (top), and *in-situ* XRD patterns collected at the INE-Beamline for the empty double containment and Pu solid phases recovered from solubility experiments at $\text{pH}_m = 9$ and 12 in hydroquinone and SnCl_2 systems ($t_{\text{eq}} = 146$ days). Squares indicate peak positions and relative intensities reported [45] for $\text{PuO}_2(\text{cr})$. Triangles correspond to peak positions and relative intensities of the double containment used for *in-situ* XRD measurements.

systems at $\text{pH}_m = 9$ and 12 ($t_{\text{eq}} = 146$ days), collected at the INE-Beamline as described in Section 2.5.2. The figure also shows the diffractogram of the empty double containment used in the synchrotron-based measurements,

as well as the XRD patterns of the starting Pu material collected with a conventional diffractometer.

Highly resolved diffractograms are obtained for all samples investigated at the INE-Beamline. A perfect match with $\text{PuO}_2(\text{cr})$ patterns previously reported [45] is obtained for the solid phases equilibrated in hydroquinone solutions, thus confirming that the initial nanocrystalline $\text{PuO}_2(\text{ncr,hyd})$ remains stable and controls the solubility of Pu in these systems. Although showing a weaker signal, a very good agreement with $\text{PuO}_2(\text{cr})$ patterns is also obtained for the solid phase recovered from the SnCl_2 system at $\text{pH}_m = 12$. Besides the pattern of $\text{PuO}_2(\text{cr})$, a number of additional reflections are observed in the SnCl_2 system at $\text{pH}_m = 9$. The latter show moderate agreement with the diffractogram of $\text{Sn}_6\text{O}_4(\text{OH})_4(\text{s})$ (PDF 14-0140) and $\text{SnO}(\text{s})$ (PDF 13-0111), which are the expected [26] solid phases controlling the solubility of Sn(II) at this pH_m . Note that Sn(II) is completely dissolved at $\text{pH}_m = 12$ due to the formation of anionic hydrolysis species, in good agreement with the lack of reflexes corresponding to Sn(II)-containing phases in the SnCl_2 buffered system at this pH_m .

These results confirm the presence of $\text{PuO}_2(\text{ncr,hyd})$ in both hydroquinone and SnCl_2 systems. Note however that both cubic $\text{Pu}_2\text{O}_3(\text{cr})$ (PDF 06328) and $\text{PuO}_{2-x}(\text{cr})$ (PDF 41-1171) share similar reflections with $\text{PuO}_2(\text{cr})$, and thus cannot be ruled out from the findings gained by XRD.

3.2.3.2 XPS

XPS spectra of solid phases recovered from the hydroquinone and SnCl_2 systems after an equilibration time of 126 days indicate the predominance of $\text{PuO}_2(\text{ncr,hyd})$ in all cases, confirming that the structure of the starting Pu material is retained. However, the spectra collected in SnCl_2 systems with $\text{pH}_m \leq 11$ exhibit poor quality, likely due to the significant presence of Sn(II)-containing phases and consequently lower Pu atomic concentration on the surface of the evaluated samples.

Note that the identification of minor contributions of other Pu redox states (e. g. +III) can be hindered by the relatively broad range of Full Width at Half-Maximum (FWHM) observed for the Pu $4f_{7/2}$ elemental lines ($2.27 \text{ eV} \leq \text{FWHM} \leq 2.87 \text{ eV}$). Variations in the FWHM can be possibly caused by structural disorder characteristic of amorphous phases, but also to inhomogeneous surface charging due to the presence of salts such as NaCl or Sn(II) oxy-hydroxides.

3.2.3.3 XANES

Pu L_{III} -edge XANES spectra collected for the solid phases controlling the solubility of Pu in hydroquinone and

SnCl_2 systems at $\text{pH}_m = 9$ and 12 are shown in Figure 5. The figure includes also the XANES spectra of the starting Pu material, as well as the reference spectra reported in Brendebach et al. [38] for aqueous Pu(III) and Pu(IV) species in acidic conditions.

The edge energies of the XANES spectra (listed in Table 2) collected for Pu solid phases in hydroquinone systems are in excellent agreement with the Pu(IV) reference spectrum [38]. Furthermore, these spectra perfectly match the XANES spectrum collected for the starting Pu material, and clearly show the existence of a PuO_2 fluorite-like structure in the analysed solid.

The shift in the white line position to lower energy ($\approx 1.2 \text{ eV}$, Figure 5) observed for Pu solid phases in SnCl_2 systems is beyond the typical energy calibration error margin ($\approx 0.5 \text{ eV}$), and unequivocally confirms a significant contribution of Pu(III). The reproduction of these spectra as a linear combination of Pu(III) and Pu(IV) reference spectra indicates an average Pu(III) content of $(30 \pm 5)\%$, both at $\text{pH}_m = 9$ and 12. Since the predominance of Pu(IV) was confirmed in the starting Pu material, this observation indicates the reduction of the initial Pu(IV) and further stabilization of Pu(III) under these (pe + pH_m) conditions. Note that a beam induced reduction in the SnCl_2 samples is ruled out accounting for the confirmed predominance of Pu(IV) in the hydroquinone samples, which were measured under exactly the same experimental conditions. Two hypotheses are considered to explain

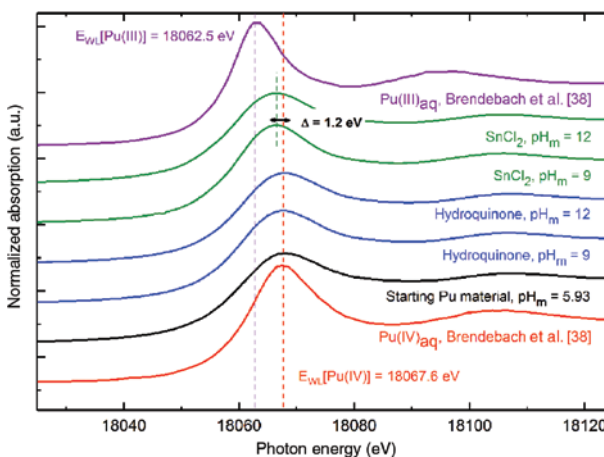


Figure 5: Pu L_{III} -edge XANES spectra of solid phases recovered from hydroquinone (blue line) and SnCl_2 systems (green line) at $\text{pH}_m = 9$ and 12 ($t_{\text{eq}} = 146$ days).

The spectra of the starting material (black) used in this study and the given references for the aqueous species of Pu(III) (purple line, position of WL = 18,062.5 eV) and Pu(IV) (red line, position of WL = 18,067.6 eV) reported in Brendebach et al. [38] are shown for comparison.

Table 2: Pu L_{III}-edge inflection points and white-line positions of the XANES spectra in Figure 5: starting Pu material used in the study, solid phases recovered from the hydroquinone and SnCl₂ systems at pH_m = 9 and 12 (t_{eq} = 146 days) and Pu(III)_{aq} and Pu(IV)_{aq} references [38].

Sample	First inflection point ^{a,b} [eV]	White line (WL) ^a [eV]
PuO ₂ (ncr,hyd), starting Pu material	18,060.3	18,068.3
Hydroquinone, pH _m = 9	18,060.9	18,067.9
Hydroquinone, pH _m = 12	18,060.7	18,068.1
SnCl ₂ , pH _m = 9	18,059.9	18,066.6
SnCl ₂ , pH _m = 12	18,059.3	18,066.7
Pu(III) _{aq} (HCl, pH=0) [38]	18,059.9	18,062.5
Pu(IV) _{aq} (HCl, pH=3) [38]	18,062.4	18,067.6
Pu(IV)(OH) ₄ (am) (sample H) [48]	18,060.5	18,068.4

^aEnergy calibration relative to first inflection point of Zr K-edge XANES assigned to 17,998 eV (E 1s) Calibration error (due to DCM motor encoder step uncertainty): ±0.5 eV.

^bNote that the position of the first inflection point is affected also by the Pu aggregation state (i. e. aqua ion vs. colloidal oxy/hydroxide species or solid precipitates).

the presence of Pu(III) in the solid phases controlling the solubility of Pu in SnCl₂ systems: (i) the coexistence of PuO₂(ncr,hyd) and Pu(OH)₃(am), or (ii) the formation of a sub-stoichiometric PuO_{2-x}(s) phase. Both options are discussed in the following sections in connection with EXAFS and solubility data.

3.2.3.4 EXAFS

The Fourier-transformed (FT) representation of the k²-weighted EXAFS data depicted in Figure 6 for hydroquinone and SnCl₂ systems (left panel: FT magnitude, imaginary part and fit results in R-space, right panel: raw data, Fourier-filtered data and fit results in k-space) corresponds to a radial pair distribution function uncorrected for photoelectron phase-shifts of the central and neighboring atoms. Two coordination shells are discernible for all samples investigated in the present work: the first one around 1.75 Å (R - Δ), which typically reflects Pu bonding to bridging oxygen atoms and to oxygen from terminal water and hydroxide units. These different oxygen neighbors, if simultaneously present in a compound, exhibit a spread of bond distances generally leading to large Debye-Waller factors or requiring inclusion of an asymmetry parameter (3rd cumulant) in the fit – or even a second oxygen neighbor shell (cf., e. g. to Rothe et al. [48]). The second shell around 3.6 Å (R - Δ) reflects backscattering from second next Pu neighbors in the solid precipitates. All metric parameters evaluated are listed in Table 3. The fit results obtained for both Pu phases

equilibrated in hydroquinone systems are almost identical and very similar to those obtained for the untreated amorphous starting material discussed in Section 3.1. The apparent disagreement between the PuO₂ fluorite-type structure observed in the XRD patterns and the reduced O and Pu coordination numbers in the Pu L_{III} EXAFS fits is actually in line with previous results obtained for Pu oxy/hydroxide phases or amorphous colloids: a rather rigid –Pu–O–Pu– ‘backbone’ or fluorite structure type lattice gives rise to the clear XRD signature, while the local order around individual Pu centers can be significantly distorted – leading to strongly reduced coordination numbers (fluorite-type PuO₂: R_{Pu–O} = 2.32 Å, N_O = 8; R_{Pu–Pu} = 3.81 Å, N_{Pu} = 12) due to destructive interference of the backscattered photoelectron waves. This discrepancy merely reflects the different sensitivity of EXAFS as a short range structural probe for order/disorder phenomena in solid materials compared to XRD, where the latter is prone to be blind to local deviations from a long range ordered structure. Interestingly, Pu samples equilibrated in SnCl₂ systems (at both pH_m values) exhibit a significant and consistent shrinking of both Pu–O and Pu–Pu distances by about 0.04–0.05 Å compared to the two hydroquinone samples (fit errors are estimated to 0.01 Å for R_{Pu–O} and 0.02 Å for R_{Pu–Pu}).

The impact of the possible coexistence of PuO₂(ncr,hyd) and Pu(OH)₃(am) on the average Pu–O distances (measured by EXAFS) in the Pu solid phases equilibrated in SnCl₂ systems is unclear. Virtually no information is available on the structure of the amorphous phase Pu(OH)₃(am), which should be probably better defined as PuO_x(OH)_{3-2x}·yH₂O(am). Pu(III)–OH bonds are expectedly shorter than Pu(IV)–O or Pu(IV)–OH₂, considering r_{OH⁻} = 1.22 Å, r_{O²⁻} = 1.40 Å and r_{OH₂⁻} = 1.38 Å reported previously [55–57]. Note, however that the number of Pu(III)–OH bonds in PuO_x(OH)_{3-2x}·yH₂O(am) is unknown and thus, the impact on the Pu–O distances cannot be properly assessed.

The shrinking of Pu–O and Pu–Pu distances in the solid phases containing Pu(III) is unexpected because of the larger size of the Pu³⁺ ion (1.12 ± 0.02 Å, CN=8) compared to Pu⁴⁺ (1.01 ± 0.02 Å, CN=9) [52]. Only a limited number of experimental studies [46, 58–62] have investigated the structure and stability of sub-stoichiometric phases PuO_{2-x}(s). Most of these studies focussed on the behavior of PuO_{2-x}(s) phases at elevated temperature, and reported the destabilization of PuO_{2-x}(s) below 300°C. Haschke et al. [60] investigated the reaction of Pu metal (both α-phase and δ-stabilized alloy) with water at 25°C, and reported the formation of several PuO_{2-x}(s) phases (PuO_{1.714}, PuO_{1.778}, PuO_{1.8} and PuO_{1.833}) besides Pu₂O₃, PuO₂

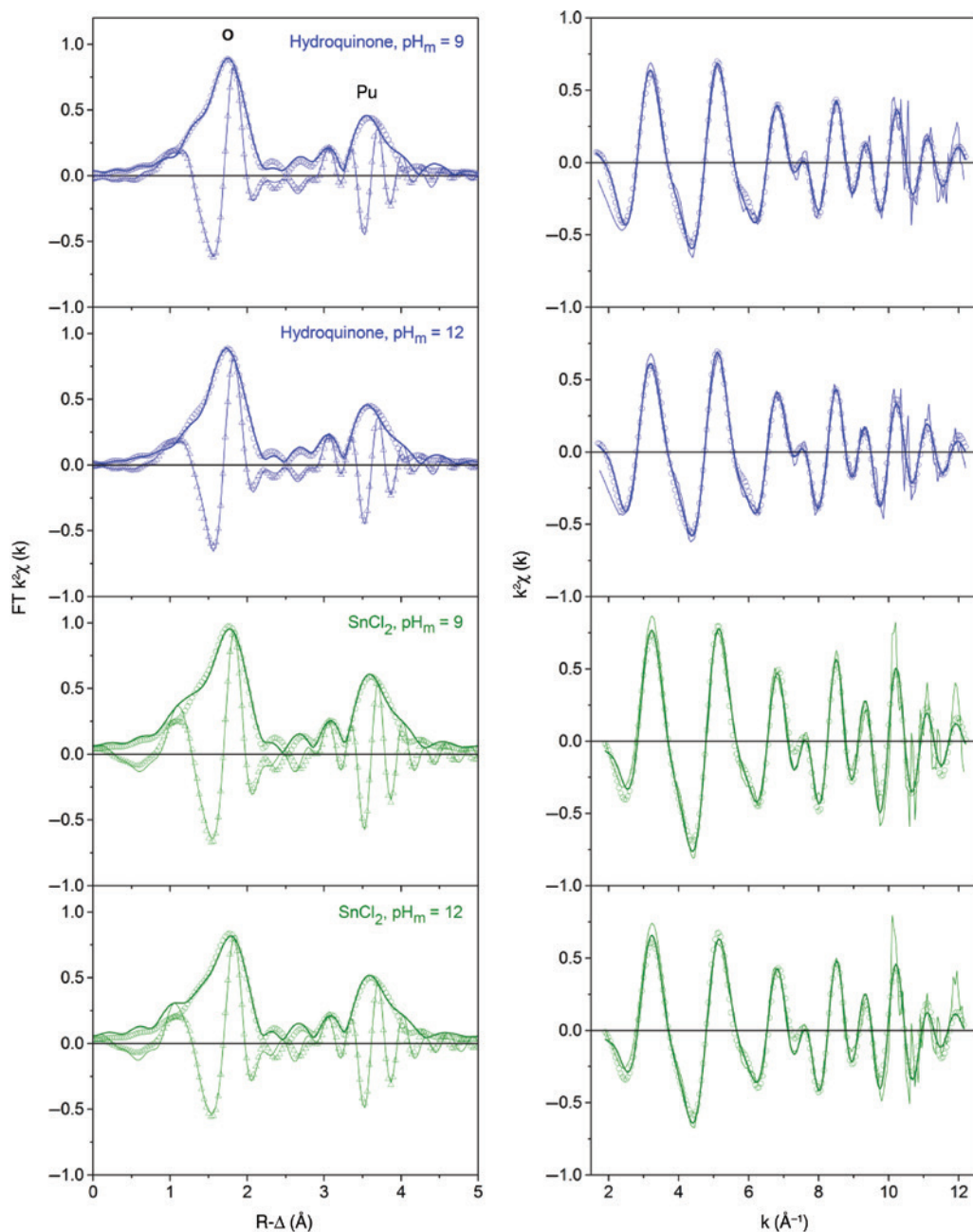


Figure 6: Pu L_{III} -edge EXAFS fit results for hydroquinone and SnCl_2 systems in R-space – left panel: FT magnitude (solid line), fit magnitude (open circles), FT real part (thin solid line) and fit real part (open triangles); right panel: Fourier-filtered data (solid line), raw data (thin solid line), back-transformed fit (open circles).

and two Pu(III) oxo-hydrides (PuOH and $\text{Pu}_7\text{O}_9\text{H}_3$). Recent publications [61, 62] by the same research team combining their own experimental results with the re-interpretation of data available in the literature concluded that the Pu–O system is not accurately described by the currently accepted Pu phase diagram, and that the formation and predominance of PuO_{2-x} (s) phases should be also expected at room temperature. Both experimental and theoretical studies report however the expansion of the

unit cell in PuO_{2-x} (s) compared to PuO_2 (s), which expectedly should correlate with an elongation of the Pu–O distance [46, 63]. It is evident from the discussion above that relevant uncertainties still affect to this system, especially in the conditions investigated in the present study, i. e. in aqueous systems at room temperature.

Although there is no doubt about the presence of up to 30% of Pu(III) in the Pu solid phases equilibrated in SnCl_2 systems, the present XAFS data cannot

Table 3: Data range and metric parameters extracted by least-squares fitting of EXAFS spectra to the EXAFS equation.

Sample	k-Range (Å ⁻¹) Fit-range (Å)	Shell	N	R (Å)	ΔE ₀ (eV)	σ ² (Å ²)	r-Factor (%)
PuO ₂ (ncr,hyd), starting Pu material	1.85–12.13	O	4.3 (8.0 ^b)	2.33	2.06 ^a	0.0046 ^c (0.0140)	2.9
	1.29–4.17	Pu	2.3	3.84		0.0004	
Pu(IV)(OH) ₄ (am) (sample H) [48]	1.71–12.5	O	4.0	2.32	2.38	0.0104	1.6
	1.35–3.99	Pu	2.4	3.87	1.84	0.0066	
Hydroquinone, pH _m = 9	1.65–12.23	O	5.2	2.32	0.09 ^a	0.0068 ^c	1.3
	1.01–4.08	Pu	3.2	3.83		0.0021	
Hydroquinone, pH _m = 12	1.60–12.10	O	5.0	2.33	2.32 ^a	0.0044 ^c	1.2
	1.01–4.08	Pu	3.2	3.83		0.0027	
SnCl ₂ , pH _m = 9	1.90–12.22	O	6.2	2.28	-1.43 ^a	0.0071 ^c	2.5
	0.83–4.17	Pu	3.7	3.78		0.0014	
SnCl ₂ , pH _m = 12	1.90–12.18	O	4.9	2.28	-1.34 ^a	0.0061 ^c	2.9
	0.83–4.17	Pu	3.2	3.78		0.0014	

S₀² = 1.0 fixed (slightly underestimating N in all fits).

^aGlobal parameter for both shells.

^bParameter fixed in fit.

^cAsymmetry parameter (3rd cumulant) applied in fit.

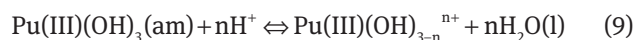
Errors: R_{Pu-O} ± 0.01 Å, R_{Pu-Pu} ± 0.02 Å.

unambiguously differentiate between the presence of two possible structural changes associated with the partial Pu(IV) reduction – either formation of a homogeneous phase, PuO_{2-x}(s), with reduced lattice constant or a mixture of predominantly fluorite type Pu(IV)O₂ and amorphous Pu(III)(OH)₃ phase. Further experimental efforts are on-going at KIT-INE to elucidate these uncertainties (see Section 3.3.2).

3.3 Thermodynamic calculations.

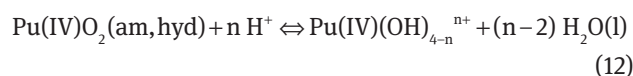
Implications of the newly generated data

Chemical reactions (9), (12) and (15) are expected to control the solubility of Pu within the experimental conditions considered in this study. The corresponding chemical equations (10, 11), (13, 14) and (16, 17) have been used in combination with stability constants and SIT ion interaction coefficients summarized in Table A1 and Table A2 of the Appendix to calculate the solubility lines in Figures 2 and 6: PuO₂(am,hyd) in equilibrium with Pu(IV)_{aq} (black line); PuO₂(am,hyd) in equilibrium with Pu(IV)_{aq} and Pu(III)_{aq} at (pe + pH_m) = 2 (gray line); and Pu(OH)₃(am) in equilibrium with Pu(III)_{aq} (green, purple and light blue lines). The three solubility curves plotted for Pu(OH)₃(am) have been calculated using log *K_{III,0}^o = 15.8, 14.35 and 14.58, as reported in NEA-TDB [5], Fellhauer [16] and Cho et al. [9], respectively.



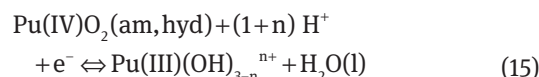
$$\log {}^*K_{\text{III},(3-n)}^{\circ} = \log {}^*K'_{\text{III},(3-n)} + \log \gamma_{\text{Pu(III)(OH)}_{3-n}{}^{n+}} + n \log a_w - n \log \gamma_{\text{H}^+} \quad (10)$$

$$\log {}^*K'_{\text{III},(3-n)} = \log m_{\text{Pu(III)(OH)}_{3-n}{}^{n+}} + n \text{pH}_m \quad (11)$$



$$\log {}^*K_{\text{IVs},(4-n)}^{\circ} = \log {}^*K'_{\text{IVs},(4-n)} + \log \gamma_{\text{Pu(IV)(OH)}_{4-n}{}^{n+}} + n \log a_w - n \log \gamma_{\text{H}^+} \quad (13)$$

$$\log {}^*K'_{\text{IVs},(4-n)} = \log m_{\text{Pu(IV)(OH)}_{4-n}{}^{n+}} + n \text{pH}_m \quad (14)$$



$$\log {}^*K_{\text{IVs/III},(3-n)}^{\circ} = \log {}^*K'_{\text{IVs/III},(3-n)} + \log \gamma_{\text{Pu(III)(OH)}_{3-n}{}^{n+}} + pe + (1+n) \log a_w - (1+n) \log \gamma_{\text{H}^+} \quad (16)$$

$$\log {}^*K'_{\text{IVs/III},(3-n)} = \log m_{\text{Pu(III)(OH)}_{3-n}{}^{n+}} + (1+n) \text{pH}_m \quad (17)$$

3.3.1 Determination of log *K_{IVs,0}^o for PuO₂(ncr,hyd) starting material

The accurate characterization of the PuO₂(ncr,hyd) solid phase and the quantification by liquid-liquid extraction of m_{Pu(IV)} in equilibrium with this phase under acidic conditions allows the quantification of log *K_{IVs,0}^o of the starting

Pu material used in the solubility experiments under alkaline to hyperalkaline pH conditions. Solid phase characterization (Section 3.2.3) has also confirmed the predominance of the same solid phase in hydroquinone systems, and thus the solubility data in this system expressed by the same $\log {}^*K_{IVs,0}^{\circ}$. The case of SnCl_2 systems, where XANES has confirmed the presence of Pu(III) in the solid phase is discussed in detail in Section 3.3.2.

Total concentration of Pu(IV) in equilibrium with $\text{PuO}_2(\text{ncr,hyd})$ at $\text{pH}_m = 3.76$ and 3.86 was quantified by liquid-liquid extraction as described in Section 3.2.2. Based on the experimentally measured $m_{\text{Pu(IV)}}$, the concentration of free $\text{Pu}^{4+}(\text{aq})$ was calculated using equation (18):

$$m_{\text{Pu}^{4+}} = m_{\text{Pu(IV)}} \cdot \left(1 + \sum ({}^*\beta'_{IV,n} m_{\text{H}^+}^{-n})\right)^{-1}, \quad (18)$$

where $\log {}^*\beta'_{IV,n}$ are the hydrolysis constants of Pu(IV) (corresponding to the reactions: $\text{Pu}^{4+} + n\text{H}_2\text{O}(\text{l}) \rightleftharpoons \text{Pu(IV)(OH)}_n^{(4-n)+} + n\text{H}^+$) corrected to 0.1 m NaCl using the SIT approach. Based on the calculated $m_{\text{Pu}^{4+}}$ and according with chemical reaction (12) for $n = 4$, the conditional solubility product of $\text{PuO}_2(\text{ncr,hyd})$ in 0.1 m NaCl ($\log {}^*K'_{IVs,0}$) can be calculated based on equation (14), and recalculated to the standard state ($\log {}^*K_{IVs,0}^{\circ}$) using equation (13).

The resulting mean value of the solubility product of the $\text{PuO}_2(\text{ncr,hyd})$ phase used in this study was determined as $\log {}^*K_{IVs,0}^{\circ} = -(58.1 \pm 0.3)$, which is in excellent agreement with the selected reference value of $-(58.3 \pm 0.5)$, reported in Neck et al. [2] and NEA-TDB [5]. The relatively large error assigned to our $\log {}^*K_{IVs,0}^{\circ}$ value arises from the uncertainty associated to the liquid-liquid extraction method.

3.3.2 On the role of Pu(III) under alkaline reducing conditions

The redox transition for the transformation $\text{PuO}_2(\text{am,hyd}) + e^- \rightleftharpoons \text{Pu(OH)}_3(\text{am})$ lays at $(\text{pe} + \text{pH}) = -(0.4 \pm 1.6)$, as calculated with the thermodynamic data (and corresponding uncertainties) currently selected in the NEA-TDB review [5]. Thus, $\text{Pu(OH)}_3(\text{am})$ is not expected to form in the $(\text{pe} + \text{pH})$ values defined by SnCl_2 systems (see Figure 1).

In contrast to the predictions by thermodynamic calculations, XANES results provide evidence on the presence of a relevant fraction of Pu(III) in the solid phases controlling the solubility of Pu in SnCl_2 systems with $\text{pH}_m = 9$ and 12 . As discussed in Section 3.2.3, the presence of Pu(III) can be explained by the coexistence of two independent solid phases of Pu(III) and Pu(IV) in the systems buffered with SnCl_2 , expectedly $\text{PuO}_2(\text{ncr,hyd})$ and $\text{Pu(OH)}_3(\text{am})$. For the simultaneous presence of two

solid phases, the phase with higher solubility (and thus less thermodynamic stability) controls the metal concentration in solution until its complete transformation into the thermodynamically stable solid phase, provided that equilibration processes between solid and liquid phase are not kinetically hindered (Ostwalds step rule). Although the solubility of $\text{Pu(OH)}_3(\text{am})$ calculated with the NEA-TDB selection [5] clearly overestimates the experimentally measured Pu solubility at $\text{pH}_m < 11$, a close inspection to the raw experimental data reported in the aforementioned studies [7, 9, 16] (see Figure 7) suggest that these results are also consistent with Pu solubility determined in the present study in SnCl_2 systems. Figure 7 shows also that all available datasets are affected by a very large dispersion, which importantly hinders the accurate description of Pu solubility phenomena under very reducing conditions.

The coexistence of two solid phases ($\text{PuO}_2(\text{ncr,hyd})$ and $\text{Pu(OH)}_3(\text{am})$) along a broad pH-range (9–12, in the present study) is feasible but unlikely from a thermodynamic point of view. It requires $\Delta_r G = 0$ within the considered $(\text{pe} + \text{pH}_m)$ boundary conditions for the chemical reaction $\text{PuO}_2(\text{ncr,hyd}) + \text{H}_2\text{O}(\text{l}) + \text{H}^+ + e^- \rightleftharpoons \text{Pu(OH)}_3(\text{am})$. This observation suggests that the coexistence of both solid phases, if confirmed, would possibly correspond to a transient state evolving towards the complete transformation into a single phase, either $\text{PuO}_2(\text{ncr,hyd})$ or $\text{Pu(OH)}_3(\text{am})$.

It is widely accepted [2, 64–68] that the fluorite-type structure of PuO_2 can easily accommodate additional oxygen atoms to charge-balance the presence of Pu(V) in $\text{PuO}_{2+x}(\text{s})$, which readily forms in the presence of traces of O_2 . A far more limited and discrepant literature is available on the formation of the sub-stoichiometric phase $\text{PuO}_{2-x}(\text{s})$. Most of the available studies [46, 58, 59] deal with dry solid material synthesized and characterized at elevated temperature (300–1000 °C), and thus are hardly comparable to the present study. The study by Haschke and co-workers [60] dealing with the corrosion of Pu metal with water at room temperature provides a somehow closer basis to compared with the material obtained in the present study. The authors could not explain their observations with the formation of either $\text{Pu(OH)}_3(\text{s})$ or $\text{PuO}_2(\text{s})$ solid phases plus H_2 , but claimed the formation of several $\text{PuO}_{2-x}(\text{s})$ phases. Unfortunately, no structural data was reported for such phases and no information on the Pu concentrations in solution were provided either.

The several experimental evidences collected in the present work (solubility, $(\text{pe} + \text{pH})$ measurements, extensive solid phase characterization, redox speciation) still do not allow us to formulate a final conclusion on the role of Pu(III) in the solid phases controlling the solubility of Pu under alkaline reducing conditions. A comprehensive

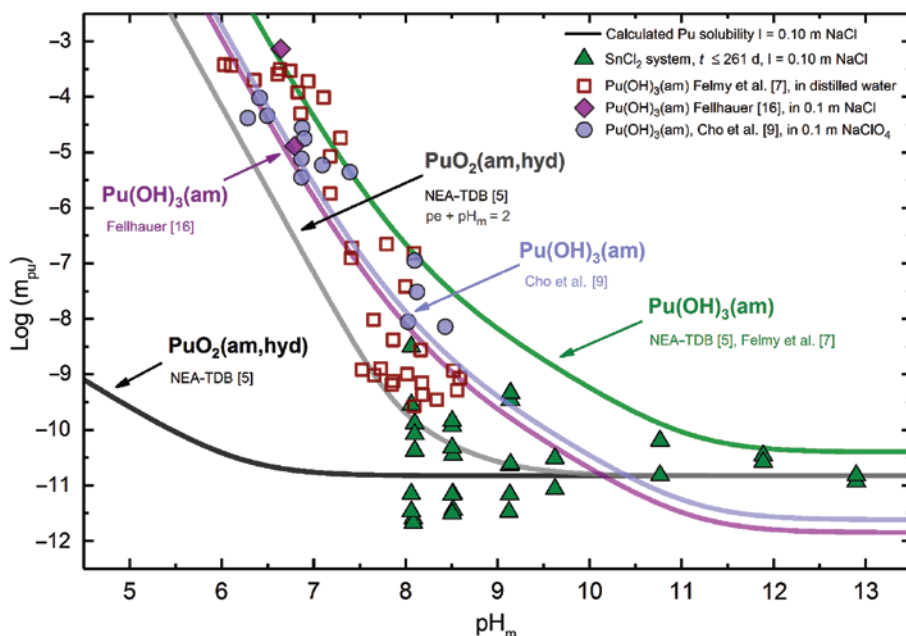


Figure 7: Plutonium total concentrations in solution in equilibrium with $\text{PuO}_2(\text{ncr,hyd})$ or $\text{Pu}(\text{OH})_3(\text{am})$ in Sn(II)-buffered systems at $I = 0.10$ m NaCl (present study, symbol: \blacktriangle), in distilled water (Felmy et al. [7], symbol: \square), in 0.10 m NaCl (Fellhauer [16], symbol: \blacklozenge), in 0.10 m NaClO_4 (Cho et al. [9], symbol: \bullet).

Solid lines correspond to the thermodynamically calculated solubility of $\text{PuO}_2(\text{am,hyd})$ in equilibrium with $\text{Pu}(\text{IV})_{\text{aq}}$ species (black line) and for $pe + pH_m = 2$ (gray line, predominance of $\text{Pu}(\text{III})_{\text{aq}}$ at $pH_m \leq 9$). Green, purple and light blue lines show the calculated solubility lines of $\text{Pu}(\text{OH})_3(\text{am})$ using $\log {}^*K_{\text{ills},0}^\circ$ values reported in NEA-TDB [5], in Fellhauer et al. [16] and in Cho et al. [9], respectively. Ionic strength corrections were performed using the SIT approach as described in Section 3.3.1.

experimental program is currently on-going at KIT-INE to elucidate the existing uncertainties: (i) characterization of the solubility and structure of $\text{Pu}(\text{OH})_3(\text{am})$ under near-neutral to weakly alkaline pH conditions, with special focus on synchrotron-based techniques (*in-situ* XRD, XAFS) at INE-Beamline; (ii) studies on long-term behavior of $\text{PuO}_2(\text{ncr,hyd})$ under very reducing conditions, with the aim of evaluating whether experimental observations in the present study correspond to thermodynamic equilibrium or to a transient state; (iii) (in collaboration with Amphos²¹ and SKB) investigation of the solubility of Pu in the presence of isosaccharinic acid (ISA) under alkaline reducing conditions. The solubility behavior of Pu(IV) and Pu(III) solid phases in the presence of strongly complexing ligands (such as ISA) is expected to provide indirect but clear insights on the character of the solid phases controlling the solubility of Pu under these boundary conditions.

4 Conclusions

The solubility and redox behavior of Pu was comprehensively investigated in acidic redox-unbuffered systems and over broad pH variations in the alkaline range under mildly and strongly reducing redox conditions. A combination of

solubility measurements, extensive solid phase characterization using a multi-method approach and Pu redox speciation analysis in both solid and aqueous phases was used to identify the solid phases and chemical equilibria controlling the solubility of Pu under ($pe + pH$) conditions relevant in the context of nuclear waste disposal. The study provides important new insight into solubility phenomena and redox processes of tetravalent and trivalent plutonium which currently is a topic of ongoing scientific debate.

A nanocrystalline $\text{PuO}_2(\text{ncr,hyd})$ solid phase was characterized using XRD, XAFS and XPS techniques and used as starting Pu material in the solubility experiments in alkaline systems buffered with hydroquinone and Sn(II). The solubility constant of this solid phase is in excellent agreement with the value of $\log {}^*K_{s,0}^\circ(\text{PuO}_2(\text{ncr,hyd}))$ currently selected in the NEA-TDB determined from independent experimental sources.

Under the mildly reducing conditions controlled by hydroquinone ($pe + pH_m = 9.5 \pm 1$), the solubility of Pu at $8 \leq pH_m \leq 13$ is very low and consistent with a solubility control by $\text{PuO}_2(\text{ncr,hyd})$. The predominance of the latter under these boundary conditions was confirmed by *in-situ* XRD, XANES and EXAFS, and is expected according to calculations using the current NEA-TDB thermodynamic data selection. XANES analyses confirm the presence of Pu(III)

in the solid phases controlling the solubility of Pu in the very reducing conditions set by Sn(II) ($p\text{e} + p\text{H}_m = 2 \pm 1$). EXAFS data further shows the shrinking of both Pu–O and Pu–Pu distances, compared to the original Pu material and $\text{PuO}_2(\text{ncr,hyd})$ equilibrated in hydroquinone systems. The solubility of Pu remains very low ($\approx 10^{-10.5}$ m) in Sn(II) systems with $p\text{H}_m \geq 9$, but shows a large scatter at $p\text{H}_m = 8$ ($\approx 10^{-9}$ – $10^{-10.5}$ m).

This work provides robust solubility upper-limits for Pu in alkaline, reducing to very reducing conditions as those expected to develop in the post-operational phase of underground repositories for the disposal of radioactive waste. It also confirms the prominent role of Pu(IV) in the solution chemistry of plutonium under mildly reducing conditions, but questions the stability range of Pu(III) solid phases in alkaline aqueous solutions predicted with the currently available thermodynamic data. Two hypotheses are proposed to explain these experimental evidences: (i) coexistence of $\text{PuO}_2(\text{ncr,hyd})$ and $\text{Pu}(\text{OH})_3(\text{am})$, and (ii) formation of a sub-stoichiometric $\text{PuO}_{2-x}(\text{s})$ phase. Further experimental efforts are on-going at KIT–INE to validate these hypotheses.

Acknowledgements: The research leading to this study was funded by SKB, the Swedish Nuclear Fuel and Waste Management Company. The contribution of Carl-Heinrich Graser (KIT–INE) in the CE–SF–ICP–MS measurements and the support from received Julian Schepperle, Nicolas Finck and Frank Heberling (all KIT–INE) in the XRD data collection and data treatment are highly appreciated. Frank Geyer and Annika Kaufmann (KIT–INE) are gratefully acknowledged for the ICP–MS measurements.

Appendix

Table A1: Thermodynamic data used for the equilibrium calculations of Pu.

Reaction	Log K°	Reference
Redox processes		
$\text{Pu}^{3+} \leftrightarrow \text{Pu}^{4+} + \text{e}^-$	$-(17.69 \pm 0.04)$	[2, 5]
$\text{Pu}^{3+} + 2\text{H}_2\text{O}(\text{l}) \leftrightarrow \text{PuO}_2(\text{am,hyd}) + 4\text{H}^+ + \text{e}^-$	$-(15.36 \pm 0.52)$	[2, 5]
$\text{Pu}^{4+} + 2\text{H}_2\text{O}(\text{l}) \leftrightarrow \text{PuO}_2^+ + 4\text{H}^+ + \text{e}^-$	$-(17.45 \pm 0.69)$	[2, 5]
$\text{PuO}_2^+ \leftrightarrow \text{PuO}_2^{2+} + \text{e}^-$	$-(15.82 \pm 0.09)$	[2, 5]
$\text{PuO}_2(\text{am,hyd}) \leftrightarrow \text{PuO}_2^+ + \text{e}^-$	$-(19.78 \pm 0.86)$	[2, 5]
Solubility and hydrolysis of Pu(III)		
$\text{Pu}(\text{OH})_3(\text{am}) \leftrightarrow \text{Pu}^{3+} + 3\text{OH}^-$	$-(26.2 \pm 1.5)^a$	[5]
$\text{Pu}^{3+} + \text{OH}^- \leftrightarrow \text{Pu}(\text{OH})^{2+}$	(7.1 ± 0.3)	[2, 5]
$\text{Pu}^{3+} + 2\text{OH}^- \leftrightarrow \text{Pu}(\text{OH})_2^+$	$(12.9 \pm 0.7)^b$	[2, 5]
$\text{Pu}^{3+} + 3\text{OH}^- \leftrightarrow \text{Pu}(\text{OH})_3^0(\text{aq})$	$(15.8 \pm 0.5)^b$	[2, 5]

Table A1 (continued)

Reaction	Log K°	Reference
Solubility and hydrolysis of Pu(IV)		
$\text{PuO}_2(\text{am, hyd}) \leftrightarrow \text{Pu}^{4+} + 4\text{OH}^-$	$-(58.33 \pm 0.52)$	[2, 5]
$\text{PuO}_2(\text{cr}) \leftrightarrow \text{Pu}^{4+} + 4\text{OH}^-$	$-(64.03 \pm 0.51)$	[2, 5]
$\text{Pu}^{4+} + \text{OH}^- \leftrightarrow \text{PuOH}^{3+}$	(14.6 ± 0.2)	[2, 5]
$\text{Pu}^{4+} + 2\text{OH}^- \leftrightarrow \text{Pu}(\text{OH})_2^{2+}$	(28.6 ± 0.3)	[2, 5]
$\text{Pu}^{4+} + 3\text{OH}^- \leftrightarrow \text{Pu}(\text{OH})_3^+$	(39.7 ± 0.4)	[2, 5]
$\text{Pu}^{4+} + 4\text{OH}^- \leftrightarrow \text{Pu}(\text{OH})_4^0(\text{aq})$	(47.5 ± 0.5)	[2, 5]
Solubility and hydrolysis of Pu(V)		
$\text{PuO}_2\text{OH}(\text{am}) \leftrightarrow \text{PuO}_2^+ + \text{OH}^-$	$-(9.0 \pm 0.5)$	[2, 5]
$\text{PuO}_{2.5}(\text{s,hyd}) \leftrightarrow \text{PuO}_2^+ + \text{OH}^-$	$-(14.0 \pm 0.5)$	[2, 5]
$\text{PuO}_2^+ + \text{OH}^- \leftrightarrow \text{PuO}_2\text{OH}^0(\text{aq})$	$(2.7 \pm 0.7)^c$	[2, 5]
$\text{PuO}_2^+ + 2\text{OH}^- \leftrightarrow \text{PuO}_2(\text{OH})_2^-$	$(4.4 \pm 0.5)^c$	[2, 5]
Solubility and hydrolysis of Pu(VI)		
$\text{PuO}_2(\text{OH})_2 \cdot \text{H}_2\text{O}(\text{s}) \leftrightarrow \text{PuO}_2^{2+} + 2\text{OH}^- + \text{H}_2\text{O}(\text{l})$	$-(22.5 \pm 1.0)$	[2, 5]
$\text{PuO}_2^{2+} + \text{OH}^- \leftrightarrow \text{PuO}_2\text{OH}^+$	(8.5 ± 0.5)	[2, 5]
$\text{PuO}_2^{2+} + 2\text{OH}^- \leftrightarrow \text{PuO}_2(\text{OH})_2^0(\text{aq})$	(14.8 ± 1.5)	[2, 5]
$\text{PuO}_2^{2+} + 3\text{OH}^- \leftrightarrow \text{PuO}_2(\text{OH})_3^-$	$(21.7 \pm 0.4)^d$	[2, 5]
$\text{PuO}_2^{2+} + 4\text{OH}^- \leftrightarrow \text{PuO}_2(\text{OH})_4^{2-}$	$(23.6 \pm 0.7)^d$	[2, 5]
$2\text{PuO}_2^{2+} + 2\text{OH}^- \leftrightarrow (\text{PuO}_2)_2(\text{OH})_2^{2+}$	(20.5 ± 1.0)	[2, 5]

^aValue is originally reported in Felmy et al. [7], but with an assigned uncertainty of ± 0.8 in \log_{10} -units.

^bIn analogy with Am(III).

^cIn analogy with Np(V).

^dIn analogy with U(VI).

Table A2: SIT ion interaction coefficients for Pu aqueous species in NaCl solutions.

I	j	$\epsilon_{ij}(\text{mol} \cdot \text{kg}^{-1})$	Reference
H^+	Cl^-	0.12 ± 0.01	[5]
Na^+	Cl^-	0.03 ± 0.01	[5]
Na^+	OH^-	0.04 ± 0.01	[5]
Pu^{3+}	Cl^-	0.23 ± 0.02	[53]
$\text{Pu}(\text{OH})_2^{2+}$	Cl^-	-0.04 ± 0.07	[53]
$\text{Pu}(\text{OH})_2^+$	Cl^-	-0.06 ± 0.08	[53]
$\text{Pu}(\text{OH})_3^0(\text{aq})$	Cl^-	0	^a
$\text{Pu}(\text{OH})_3^0(\text{aq})$	Na^+	-0.17 ± 0.10	[53]
Pu^{4+}	Cl^-	0.4 ± 0.1	[52]
PuOH^{3+}	Cl^-	0.2 ± 0.1	[52]
$\text{Pu}(\text{OH})_2^{2+}$	Cl^-	0.1 ± 0.1	[52]
$\text{Pu}(\text{OH})_3^+$	Cl^-	0.05 ± 0.1	[52]
$\text{Pu}(\text{OH})_4^0(\text{aq})$	Na^+/Cl^-	0	^a
PuO_2^+	Cl^-	0.09 ± 0.05^b	[5]
$\text{PuO}_2\text{OH}(\text{aq})$	Na^+/Cl^-	0	^a
$\text{PuO}_2(\text{OH})_2^-$	Na^+	-0.01 ± 0.07^b	[5]
PuO_2^{2+}	Cl^-	0.21 ± 0.02^c	[5]
PuO_2OH^+	Cl^-	0.05 ± 0.1^c	[69]
$\text{PuO}_2(\text{OH})_2(\text{aq})$	Na^+/Cl^-	0	^a
$\text{PuO}_2(\text{OH})_3^-$	Na^+	-0.20 ± 0.02^d	[54]
$\text{PuO}_2(\text{OH})_4^{2-}$	Na^+	-0.12 ± 0.01^d	[54]
$(\text{PuO}_2)_2(\text{OH})_2^{2+}$	Cl^-	0.69 ± 0.07^c	[5]

^aBy definition in SIT.

^bIn analogy with Np(V).

^cIn analogy with U(VI).

^dIn analogy with Np(VI).

References

- SKB: Safety Analysis SFR 1. Long-Term Safety (2008), Svensk Kärnbränslehantering AB, Stockholm, Sweden.
- Neck, V., Altmaier, M., Fanghänel, T.: Solubility of plutonium hydroxides/hydrous oxides under reducing conditions and in the presence of oxygen. *C. R. Chim.* **10**, 959 (2007).
- Grenthe, I., Fuger, J., Lemire, R. J., Muller, A. B., Cregu, C. N., Wanner, H.: *Chemical Thermodynamics, Vol. 1. Chemical Thermodynamics of Uranium (1992)*, OECD, NEA-TDB, Elsevier, North Holland, Amsterdam.
- Lemire, R. J., Fuger, J., Nitsche, H., Potter, P. E., Rand, M. H., Rydberg, J., Spahi, K., Sullivan, J. C., Ullman, W. J., Vitorge, P., Wanner, H.: *Chemical Thermodynamics, Vol. 4. Chemical Thermodynamics of Neptunium and Plutonium (2001)*, OECD, NEA-TDB, Elsevier, North Holland, Amsterdam.
- Guillaumont, R., Fanghänel, T., Neck, V., Fuger, J., Palmer, D. A., Grenthe, I., Rand, M. H.: *Chemical Thermodynamics, Vol. 5. Update on the Chemical Thermodynamics of Uranium, Neptunium, Plutonium, Americium and Technetium (2003)*, OECD, NEA-TDB, Elsevier, North Holland, Amsterdam.
- Altmaier, M., Neck, V., Lützenkirchen, J., Fanghänel, T.: Solubility of plutonium in MgCl₂ and CaCl₂ solutions in contact with metallic iron. *Radiochim. Acta* **97**, 187 (2009).
- Felmy, A. R., Rai, D., Schramke, J. A., Ryan, J. L.: The solubility of plutonium hydroxide in dilute solution and in high-ionic-strength chloride brines. *Radiochim. Acta* **48**, 29 (1989).
- Nilsson, H.: *The Chemistry of Plutonium Solubility*, Ph.D. Thesis, Chalmers University of Technology (Nuclear Chemistry, Department of Materials and Surface Chemistry), Göteborg, Sweden (2004).
- Cho, H. R., Youn, Y. S., Jung, E. C., Cha, W.: Hydrolysis of trivalent plutonium and solubility of Pu(OH)₃ (am) under electrolytic reducing conditions. *Dalton Trans.* **45**, 19449 (2016).
- Fujiwara, K., Yamana, H., Fujii, T., Moriyama, H.: Solubility product of plutonium hydrous oxide. *J. Nucl. Fuel Cycle Environ. (Jpn.)* **7**, 17 (2001).
- Fujiwara, K., Yamana, H., Fujii, T., Moriyama, H.: Solubility product of plutonium hydrous oxide and its ionic strength dependence. *Radiochim. Acta* **9**, 857 (2002).
- Rai, D., Gorby, Y. A., Fredrickson, J. K., Moore, D. A., Yui, M.: Reductive dissolution of PuO₂(am): the effect of Fe(II) and hydroquinone. *J. Solution Chem.* **31**, 433 (2002).
- Kraus, K. A., Dam, J. R.: Hydrolytic Behavior of Plutonium (III) Acid-Base Titrations of Plutonium (III). Technical Report, AECD-2543 (CN-2832) (1945).
- Hubert, S., Hussonnois, M., Guillaumont, R.: [Comportement du plutonium trivalent lors de son extraction par la thenoyltrifluoroacetone](#). *J. Inorg. Nucl. Chem.* **37**, 1255 (1975).
- Nair, G. M., Chander, K., Joshi, J. K.: Hydrolysis constants of plutonium(III) and americium(III). *Radiochim. Acta* **30**, 37 (1982).
- Fellhauer, D.: *Untersuchungen zur Redoxchemie und Löslichkeit von Neptunium und Plutonium*, PhD-thesis, Ruprecht-Karls-Universität Heidelberg, Heidelberg, Germany (2013).
- Powell, B. A., Fjeld, R. A., Kaplan, D. I., Coates, J. T., Serkiz, S. M.: Pu(V)O₂ + adsorption and reduction by synthetic magnetite (Fe₃O₄). *Environ. Sci. Technol.* **38**, 6016 (2004).
- Powell, B. A., Duff, M. C., Kaplan, D. I., Fjeld, R. A., Newville, M., Hunter, D. B., Bertsch, P. M., Coates, J. T., Eng, P., Rivers, M. L., Serkiz, S. M., Sutton, S. R., Triay, I. R., Vaniman, D. T.: Plutonium oxidation and subsequent reduction by Mn(IV) minerals in Yucca Mountain tuff. *Environ. Sci. Technol.* **40**, 3508 (2006).
- Kirsch, R., Fellhauer, D., Altmaier, M., Neck, V., Rossberg, A., Fanghänel, T., Charlet, L., Scheinost, A. C.: Oxidation state and local structure of plutonium reacted with magnetite, mackinawite, and chukanovite. *Environ. Sci. Technol.* **45**, 7267 (2011).
- Felmy, A. R., Moore, D. A., Rosso, K. M., Qafoku, O., Rai, D., Buck, E. C., Ilton, E. S.: Heterogeneous reduction of PuO₂ with Fe(II): importance of the Fe(III) reaction product. *Environ. Sci. Technol.* **45**, 3952 (2011).
- Felmy, A. R., Moore, D. A., Pearce, C. I., Conradson, S. D., Qafoku, O., Buck, E. C., Rosso, K. M., Ilton, E. S.: Controls on soluble Pu concentrations in PuO₂/magnetite suspensions. *Environ. Sci. Technol.* **46**, 11610 (2012).
- Felmy, A. R., Moore, D. A., Qafoku, O., Buck, E., Conradson, S. D., Ilton, E. S.: Heterogeneous reduction of ²³⁹PuO₂ by aqueous Fe(II) in the presence of hematite. *Radiochim. Acta* **101**, 701 (2013).
- González-Siso, M. R., Gaona, X., Duro, L., Schild, D., Fellhauer, D., Pidchenko, I., Vitova, T., Altmaier, M., Bruno, J.: Interaction of Pu, U and Tc with iron corrosion products under hyperalkaline reducing conditions. 15th International Conference on the Chemistry and Migration Behaviour of Actinides and Fission Products in the Geosphere, MIGRATION 2015, Abstract book, p. 329 (2015).
- Altmaier, M., Metz, V., Neck, V., Müller, R., Fanghänel, T.: Solid-liquid equilibria of Mg(OH)₂(cr) and Mg₂(OH)₃Cl · 4H₂O(cr) in the system Mg-Na-H-OH-Cl-H₂O at 25°C. *Geochim. Cosmochim. Acta* **67**, 3595 (2003).
- Altmaier, M., Gaona, X., Fellhauer, D., Buckau, G.: FP7 EURATOM Collaborative Project “Redox Phenomena Controlling Systems” Intercomparison of redox determination methods on designed and near-natural aqueous systems, KIT Scientific Reports 7572, Karlsruhe, Germany (2010).
- Gamsjäger, H., Gajda, T., Sangster, J., Saxena, S. K., Voigt, W., *Chemical Thermodynamics Series, Vol. 12. Chemical Thermodynamics of Tin (2012)*, NEA-TDB, Elsevier, North Holland, Amsterdam.
- Yalcintas, E., Gaona, X., Scheinost, A. C., Kobayashi, T., Altmaier, M., Geckeis, H.: Redox chemistry of Tc(VII)/Tc(IV) in dilute to concentrated NaCl and MgCl₂ solutions. *Radiochim. Acta* **103**, 57 (2015).
- Kobayashi, T., Scheinost, A. C., Fellhauer, D., Gaona, X., Altmaier, M.: Redox behavior of Tc(VII)/Tc(IV) under various reducing conditions in 0.1M NaCl solutions. *Radiochim. Acta* **101**, 323 (2013).
- Akatsu, J.: Separation of plutonium-238 from fission products by solvent extraction using HDEHP. *J. Nucl. Sci. Technol.* **10**, 696 (1973).
- Nitsche, H., Lee, S. C., Gatti, R. C.: [Determination of plutonium oxidation states at trace levels pertinent to nuclear waste disposal](#). *J. Radioanal. Nucl. Chem.* **124**, 171 (1988).
- Schramke, J. A., Rai, D., Fulton, R. W., Choppin, G. R.: [Determination of aqueous plutonium oxidation states by solvent extraction](#). *J. Radioanal. Nucl. Chem.* **130**, 333 (1989).
- Nitsche, H., Roberts, K., Xi, R., Prussin, T., Becraft, K., Al Mahamid, I., Silber, H., Carpenter, S. A., Gatti, R. C., Novak, C. F.: Long term plutonium solubility and speciation studies in a synthetic brine. *Radiochim. Acta* **66**, 3 (1994).

33. Manchanda, V. K., Mohapatra, P. K.: 1-Phenyl-3-methyl-4-benzoyl-pyrazolone-5: a promising extractant for plutonium. *Sep. Sci. Technol.* **29**, 1073 (1994).
34. Graser, C. H., Banik, N. L., Bender, K. A., Lagos, M., Marquardt, C. M., Marsac, R., Montoya, V., Geckeis, H.: Sensitive redox speciation of iron, neptunium, and plutonium by capillary electrophoresis hyphenated to inductively coupled plasma sector field mass spectrometry. *Anal. Chem.* **87**, 9786 (2015).
35. Joint Committee on Powder Diffraction Standards: JCPDS-Powder Diffraction Files (2001), Swarthmore, USA.
36. Rothe, J., Butorin, S., Dardenne, K., Denecke, M. A., Kienzler, B., Loble, M., Metz, V., Seibert, A., Steppert, M., Vitova, T., Walther, C., Geckeis, H.: [The INE-Beamline for actinide science at ANKA](#). *Rev. Sci. Instrum.* **83**, 043105 (2012).
37. Ravel, B., Newville, M.: ATHENA, ARTEMIS, HEPHAESTUS: data analysis for X-ray absorption spectroscopy using IFEFFIT. *J. Synchrotron Radiat.* **12**, 537 (2005).
38. Brendebach, B., Banik, N. L., Marquardt, C. M., Rothe, J., Denecke, M., Geckeis, H.: X-ray absorption spectroscopic study of trivalent and tetravalent actinides in solution at varying pH values. *Radiochim. Acta* **97**, 701 (2009).
39. Walther, C., Rothe, J., Brendebach, B., Fuss, M., Altmaier, M., Marquardt, C. M., Büchner, S., Cho, H.-R., Yun, J. I., Seibert, A.: New insights in the formation processes of Pu(IV) colloids. *Radiochim. Acta* **97**, 199 (2009).
40. Stern, E. A., Newville, M., Ravel, B., Yacoby, Y., Haskel, D.: The UWXAFS analysis package – philosophy and details. *Physica B* **209**, 117 (1995).
41. Ankudinov, A. L., Ravel, B., Rehr, J. J., Conradson, S. D.: [Real-space multiple-scattering calculation and interpretation of X-ray absorption near-edge structure](#). *Phys. Rev. B* **58**, 7565 (1998).
42. De Nolf, W., Vanmeert, F., Janssens, K.: XRDU: crystalline phase distribution maps by two-dimensional scanning and tomographic (micro) X-ray powder diffraction. *J. Appl. Crystallogr.* **47**, 1107 (2014).
43. Smrcok, L.: Rietveld refinement of Y2O3, using the Pearson VII profile shape function. *Cryst. Res. Technol.* **24**, 607 (1989).
44. Seah, M. P., Gilmore, L. S., Beamson, G.: XPS: binding energy calibration of electron spectrometers 5 – re-evaluation of the reference energies. *Surf. Interface Anal.* **26**, 642 (1998).
45. Zachariassen, W. H.: Crystal chemical studies of the 5f-series of elements. XII. New compounds representing known structure types. *Acta Crystallogr.* **2**, 388 (1949).
46. Gardner, E. R., Markin, T. L., Street, R. S.: [The plutonium-oxygen phase diagram](#). *J. Inorg. Nucl. Chem.* **27**, 541 (1965).
47. Rothe, J., Walther, C., Brendebach, B., Büchner, S., Fuss, M., Denecke, M. A., Geckeis, H.: A combined XAFS, ESI TOF-MS and LIBD study on the formation of polynuclear Zr(IV), Th(IV) and Pu(IV) species. *J. Phys. Conf. Ser.* **190**, 012188 (2009).
48. Rothe, J., Walther, C., Denecke, M., Fanghaenel, T.: XAFS and LIBD investigation of the formation and structure of colloidal Pu(IV) hydrolysis products. *Inorg. Chem.* **43**, 4708 (2004).
49. Courteix, D., Chayrouse, J., Heintz, L., Baptist, R.: XPS study of Pu oxides. *Solid State Commun.* **39**, 209 (1981).
50. Larson, D. T., Haschke, J. M.: XPS-AES characterization of plutonium oxides and oxide carbide. The existence of plutonium monoxide. *Inorg. Chem.* **20**, 1945 (1981).
51. Cox, L. E., Farr, J. D.: 4f-binding-energy shifts of the light-actinide dioxides and tetrafluorides. *Phys. Rev. B* **39**, 11142 (1989).
52. Neck, V., Kim, J. I.: [Solubility and hydrolysis of tetravalent actinides](#). *Radiochim. Acta* **89**, 1–16 (2001).
53. Neck, V., Altmaier, M., Rabung, T., Lützenkirchen, J., Fanghänel, T.: Thermodynamics of trivalent actinides and neodymium in NaCl, MgCl2, and CaCl2 solutions: solubility, hydrolysis, and ternary Ca-M(III)-OH complexes. *Pure Appl. Chem.* **81**, 1555 (2009).
54. Gaona, X., Fellhauer, D., Altmaier, M.: Thermodynamic description of Np(VI) solubility, hydrolysis, and redox behavior in dilute to concentrated alkaline NaCl solutions. *Pure Appl. Chem.* **85**, 2027 (2013).
55. Gaona, X., Tits, J., Dardenne, K., Liu, X., Rothe, J., Denecke, M. A., Wieland, E., Altmaier, M.: Spectroscopic investigations of Np(V/VI) redox speciation in hyperalkaline TMA-(OH, Cl) solutions. *Radiochim. Acta* **100**, 759 (2012).
56. Shannon, R. D.: [Revised effective ionic radii and systematic studies of interatomic distances in halides and chalcogenides](#). *Acta Crystallogr. A* **32**, 751 (1976).
57. Marcus, Y.: Thermodynamics of solvation of ions. *J. Chem. Soc. Faraday Trans.* **87**, 2995 (1991).
58. McNeilly, C. E.: The electrical properties of plutonium oxides. *J. Nucl. Mater.* **11**, 53 (1964).
59. Atlas, L. M., Schlehman, G. J., Readey, D. W.: Defects in PuO2-x: density measurements at high temperature. *J. Am. Ceram. Soc.* **49**, 624 (1966).
60. Haschke, J. M., Hodges, A. E., Bixby, G. E., Lucas, R. L.: *The Reaction of Plutonium with Water: Kinetic and Equilibrium Behavior of Binary and Ternary Phases in the Pu + O + H System* (1983), G.A. Riordan, Albuquerque Operations Office, U.S. Department of Energy, Golden, Colorado, USA.
61. Dinh, L. N., Haschke, J. M., Saw, C. K., Allen, P. G., McLean, W.: Pu2O3 and the plutonium hydriding process. *J. Nucl. Mater.* **408**, 171 (2011).
62. Haschke, J. M., Dinh, L. N., McLean, W.: The plutonium–oxygen phase diagram in the 25–900°C range: non-existence of the PuO1.515 phase. *J. Nucl. Mater.* **458**, 275 (2015).
63. Petit, L., Svane, A., Szotek, Z., Temmerman, W. M., Stocks, G. M.: [Electronic structure and ionicity of actinide oxides from first principles](#). *Phys. Rev. B* **81**, 045108 (2010).
64. Haschke, J. M., Allen, T. H., Morales, L. A.: Reaction of plutonium dioxide with water: formation and properties of PuO2 + x. *Science* **287**, 285 (2000).
65. Conradson, S. D., Begg, B. D., Clark, D. L., Den Auwer, C., Espinosa-Faller, F. J., Gordon, P. L., Hess, N. J., Hess, R., Webster Keogh, D., Morales, L. A., Neu, M. P., Runde, W., Tait, C. D., Veirs, D. K., Vilella, P. M.: Speciation and unusual reactivity in PuO2 + x. *Inorg. Chem.* **42**, 3715 (2003).
66. Neck, V., Altmaier, M., Seibert, A., Yun, J. I., Marquardt, C. M., Fanghänel, T.: Solubility and redox reactions of Pu(IV) hydrous oxide: evidence for the formation of PuO2 + x(s, hyd). *Radiochim. Acta* **95**, 193 (2007).
67. Neck, V., Altmaier, M., Fanghänel, T.: Thermodynamic data for hydrous and anhydrous PuO2 + x(s). *J. Alloys Compd.* **444–445**, 464 (2007).
68. Petit, L., Svane, A., Szotek, Z., Temmerman, W. M.: [First-principles calculations of PuO2 + x](#). *Science* **301**, 498 (2003).
69. Hummel, W.: *Ionic Strength Corrections and Estimation of SIT Ion Interaction Coefficients* (2009), P.S. Institut, Villigen, Switzerland.